Annual Cycle and ENSO in a Coupled Ocean–Atmosphere General Circulation Model

EDWIN K. SCHNEIDER, ZHENGXIN ZHU, BENJAMIN S. GIESE, HUANG, BEN P. KIRTMAN, J. SHUKLA, AND JAMES A. CARTON†

Center for Ocean–Land–Atmosphere Studies, Calverton, Maryland

(Manuscript received 8 May 1995, in final form 31 October 1995)

ABSTRACT

Results from multiyear integrations of a coupled ocean–atmosphere general circulation model are described. The atmospheric component is a rhomboidal 15, 18-level version of the Center for Ocean–Land–Atmosphere Studies atmospheric general circulation model. The oceanic component is the Geophysical Fluid Dynamics Laboratory ocean model with a horizontal domain extending from 70°S to 65°N. The ocean model uses 1.5° horizontal resolution, with meridional resolution increasing to 0.5° near the equator, and 20 vertical levels, most in the upper 300 m. No flux adjustments are employed.

An initial multiyear integration showed significant climate drift in the tropical Pacific sea surface temperatures. Several modifications were made in the coupled model to reduce these errors. Changes were made to the atmospheric model cloudiness parameterizations, increasing solar radiation at the surface in the western equatorial Pacific and decreasing it in the eastern Pacific, that improved the simulation of the time-mean sea surface temperature. Large errors in the wind direction near the western coast of South America resulted in large mean SST errors in that region. A procedure to reduce these errors by extrapolating wind stress values away from the coast to coastal points was devised and implemented.

Results from the last 17 years of a 62-yr simulation are described. The model produces a reasonably realistic annual cycle of equatorial Pacific sea surface temperature. However, the upper-ocean thermal structure has serious errors. Interannual variability for tropical Pacific sea surface temperatures, precipitation, and sea level pressure that resemble the observed El Niño–Southern Oscillation (ENSO) in structure and evolution is found. However, differences from observed behavior are also evident. The mechanism responsible for the interannual variability appears to be similar to the delayed oscillator mechanism that occurs in the real climate system.

The structure of precipitation, sea level pressure, and geopotential anomalies associated with the tropical Pacific sea surface temperature interannual variability are isolated and described. The coupled model is capable of producing structures that are similar to those observed.

It is concluded that atmosphere–ocean general circulation models are beginning to capture some of the observed characteristics of the climatology of the tropical Pacific and the interannual variability associated with the El Niño–Southern Oscillation. Remaining obstacles to realistic simulations appear to include ocean model errors in the eastern equatorial Pacific, errors associated with cloud–radiation interactions, and perhaps errors associated with inadequate meridional resolution in the atmospheric model equatorial Pacific.

1. Introduction

This paper describes results from an extended integration of a coupled ocean–atmosphere general circulation model. The analysis focuses on the annual cycle and interannual variability in the tropical Pacific, and the global repercussions of this interannual variability. The aim is to document the strengths and weaknesses of a coupled ocean–atmosphere model in order to establish a baseline for evaluating future modifications and for comparison with other models.

Coupled atmosphere–ocean general circulation models (GCM) are being developed for simulating and predicting tropical and extratropical climate variability associated with the El Niño–Southern Oscillation (ENSO). This phenomenon has been the object of intensive study during the recently completed TOGA (Tropical Ocean Global Atmosphere) experiment. An important verification of the realism of the model formulations and physical parameterizations is the ability of these models to simulate both the annual cycle of sea surface temperature (SST) and the statistics of the interannual ENSO variability in the tropical Pacific. Initial attempts, reviewed by Neelin et al. (1992), were unsuccessful in qualitatively simulating one or both phenomena. Philander et al. (1992) produced realistic ENSO variability

* Current affiliation: Department of Oceanography, Texas A&M University, College Station, Texas.

† Current affiliation: Department of Meteorology, University of Maryland, College Park, Maryland.

Corresponding author address: Dr. Edwin K. Schneider, Center for Ocean–Land–Atmosphere Studies, Powder Mill Road, Suite 302, Calverton, MD 20705.
E-mail: schneide@cola.iges.org

but contained no simulation of the annual cycle. Interannual variability in the tropical Pacific was weak or absent in many of the other coupled GCMs. Additionally, some coupled GCM simulations exhibited systematic eastward or westward propagation of SST anomalies, in contrast to observations. Many of the other simulations described in Neelin et al. (1992) were so poor that coupled GCMs seemed at the time to be uncompetitive with coupled models of intermediate complexity (e.g., Cane and Zebiak 1987) for practical applications.

Mechoso et al. (1995) compared the annual cycles over the tropical Pacific of a number of coupled GCMs, including the one that is the subject of this article, to observations. Many flaws were evident in the simulated SST and precipitation.

Some progress in the joint simulation of the tropical annual cycle and interannual variability, compared to the results described in Neelin et al. (1992), has been demonstrated by Nagai et al. (1992), Latif et al. (1993, 1994), and Robertson et al. (1995a,b). These simulations all developed annual cycles or interannual variability of tropical Pacific SST that is realistic to some extent. However, serious problems were still noticeable.

Since the climatologies of the coupled GCMs must still be considered poor, the strategy of anomaly coupling has been adopted for dynamical prediction of interseasonal and interannual tropical Pacific SST anomalies with coupled GCMs (Ji et al. 1994; Kirtman et al. 1997). This procedure controls the climatology of a coupled model by specifying the observed annual cycle of SST for forcing the atmospheric GCM. The observed annual cycle of wind stress and heat flux are specified for forcing the ocean GCM. Two-way interactive coupling is allowed for interannual timescales, but the anomalies may be subject to empirical statistical corrections. Anomaly coupling effectively creates a new class of coupled model that is computationally more complex, but philosophically closer to an intermediate coupled model, than a full coupled GCM. By controlling departures of the coupled model climatology and anomalies from reality, anomaly coupling allows skillful predictions to be made for tropical Pacific SST anomalies. But anomaly coupling does not remove the root causes of the model problems, which must be due to inaccurate parameterizations or numerics, and these inaccuracies will also produce noncorrectable errors in the prediction of the anomalies. It is logical to expect that better predictions can be made when the causes of the poor simulations are eliminated, making anomaly coupling no longer necessary. To improve the fully coupled GCMs, simulations from these models must be analyzed and the inaccurate parameterizations and numerics found and corrected.

We describe below the results from 62 years of simulation with a coupled GCM. The domain of the ocean GCM is nearly global, excluding the regions near the poles. The atmospheric model horizontal resolution is the same as the atmospheric model used by Lau et al. (1992) and Philander et al. (1992), while twice the number of levels in the vertical are employed in this work. The ocean model is the same used by Lau et al. (1992), Philander et al. (1992), and Robertson et al. (1995a,b). The ocean model resolution is slightly less than that used by Philander et al. (1992) and Robertson et al. (1995a,b) in their Pacific basin ocean models. The domain is nearly the same as in Lau et al. (1992), which used a lower horizontal resolution version of the ocean model. Several changes were made after testing the coupled model in an attempt to improve the simulation of the annual mean tropical Pacific SST. The adjustments to the physical parameterizations included tuning of the radiative properties of convective and stratus clouds, and empirically correcting wind direction near the eastern boundaries of the tropical ocean. The annual cycle and interannual variability of the tropical Pacific are described for the last 17 years of the simulation, after the model has approached an equilibrium climate. The simulation verifies against observations comparably to the results described by Nagai et al. (1992), Latif et al. (1993, 1994), and Robertson et al. (1995a,b); however, the magnitude of anomalies from the annual cycle of equatorial Pacific SST is only about half of that observed in recent decades. The SST anomalies found in the Philander et al. (1992) simulation are stronger, which is more realistic. The mechanism for interannual variability of the equatorial Pacific SST is shown to be related to the delayed oscillator mechanism (Schopf and Suarez 1988; Suarez and Schopf 1988; Battisti and Hirst 1989). The weakness of the simulated interannual variability appears to be connected to weakness in the simulated Rossby wave link in the western Pacific. Despite the relatively weak interannual variability of equatorial Pacific SST, the model simulates ENSO-related global atmospheric patterns that bear some resemblance to those observed.

2. Model description

The elements of the coupled model are the Center for Ocean–Land–Atmosphere Studies (COLA) atmospheric general circulation model (AGCM) and the Geophysical Fluid Dynamics Laboratory (GFDL) modular ocean model (MOM), version 1.0. These are briefly described below. The coupling between the atmosphere and ocean is direct—no flux correction is applied. An initial multiyear integration of the coupled model revealed large systematic errors in tropical Pacific sea surface temperatures. Changes made to the atmospheric model cloud–radiation interaction parameterizations and the coupling procedure to improve the model performance are described below.

a. The atmosphere and land surface models

The atmospheric model used in all the experiments described herein is the Center for Ocean–Land–Atmo-

sphere Studies AGCM. The dynamical core of the model (Kinter et al. 1988) is based on the National Centers for Environmental Prediction (formerly known as the National Meteorological Center, NMC) global spectral model developed for medium-range weather forecasting (Sela 1980). The biophysically based land surface parameterization (Xue et al. 1991) is a simplification of the SiB parameterization (Sellers et al. 1986; Sato et al. 1989a). The atmosphere–land surface model used in these experiments is the same as that presented by Xue et al. (1991), except that an interactive cloud–radiation scheme was added (Hou 1990; after Slingo 1987). Some modifications to the cloud–radiation interaction, described in section 2d, were implemented beginning in the third year of the simulation.

The horizontal resolution of the version of the AGCM used in this study is rhomboidal truncation at wavenumber 15. The vertical structure of the model is represented by 18 unevenly spaced levels using sigma (Phillips 1957) as the vertical coordinate. The layer depths as a fraction of the total atmospheric mass from the ground up are 0.01, 0.017, 0.025, 0.055, 0.073, 0.085, 0.093, 0.096, and 0.096 for the lower nine levels. The upper nine layers have constant mass fraction 0.05. The spacing of the levels is the same as that used in Kinter et al. (1988). The AGCM includes parameterizations of solar radiative heating (Lacis and Hansen 1974); terrestrial radiative heating (Harshvardhan et al. 1987); cloud–radiation interaction as mentioned above; deep convection (a modification of Kuo 1965); shallow convection (Tiedtke 1984); large-scale condensation (relative humidity criterion as in Sela 1980); gravity wave drag (Vernekar et al. 1992; after Alpert et al. 1988); a turbulence closure scheme for subgrid-scale exchanges of heat, momentum, and moisture (Miyakoda and Sirutis 1977; after Mellor and Yamada 1982, level 2.0); and biophysically controlled interactions between the vegetated land surface and the atmosphere as mentioned above. An approximate fit to the Monin–Obukhov similarity theory for the surface transfer coefficients (Miyakoda and Sirutis 1977) is used over the oceans (Sato et al. 1989b), with a minimum surface wind speed of 2 m s^{-1}.

Since mass is not conserved due to spectral truncation, the surface pressure is adjusted uniformly over the globe once daily to guarantee that the total mass of the atmosphere remains approximately constant. Moisture is borrowed from the underlying atmospheric layer to restore the humidity in a layer to zero if specific humidity in that layer becomes negative (following ECMWF 1988). Both schemes are described in Schneider and Kinter (1994).

Boundary conditions applied at the lower surface of the AGCM include the specification of SST, sea ice extent, and surface albedo of the oceans. The SST seen by the atmosphere is the observed SST plus a spatially dependent, time-independent term that corrects for the spectral truncation error that produces nonzero elevation of the lower boundary of the atmosphere over the ocean (K. Campana and M. Kanamitsu 1988, personal communication). The correction has the value $-6.5z_{atm}$ K, where z_{atm} (km) is the height of the atmospheric lower boundary. The initial snow depth is specified, and the model predicts the snow depth after the initial time. Surface stress over the ocean is computed assuming zero surface current. The topographic elevation is a smoothed mean orography (Fennessy et al. 1994). The initial conditions applied to the AGCM were based on National Meteorological Center (NMC) global analyses for 1 January 1987.

b. The ocean model

The ocean model used in the coupled integration was adapted from the GFDL modular ocean model (Bryan and Lewis 1979). This model is a finite-difference treatment of the primitive equations of motion on the sphere. Nonlinear vertical mixing of heat, salinity, and momentum (Pacanowski and Philander 1981) and constant coefficient horizontal mixing of heat and momentum with a mixing coefficient of 2×10^7 cm^2 s^{-1} were chosen. Sunlight is assumed to penetrate the upper surface with an *e*-folding depth of 12 m. No parameterization of sea ice formation or transport is included.

The ocean model zonal resolution was chosen to be 1.5° longitude. A varying meridional resolution was taken for enhanced resolution in the equatorial waveguide. The meridional grid spacing is 0.5° between 10°N and 10°S, increasing to 1.5° poleward of 20°N and 20°S. There are 20 layers in the vertical with a maximum depth of 4000 m. The top 10 layers are each 15 m in depth. The depths of the lower 10 layers, from the top down, are 15.2, 16.1, 20.0, 34.1, 75.9, 177.1, 375.9, 687.4, 1063.8, and 1384.5 m. We begin with realistic basin boundaries and bathymetry for the world oceans between 70°S and 65°N, derived from the Scripps 1° × 1° topography dataset that is part of the MOM database. Then, ocean depths less than 100 m are set to 100 m. Also, the boundaries are simplified to reduce the number of islands. In addition to the large continents, there are five resolved islands: Antarctica, Australia, Madagascar, Borneo, and Java. The Indonesian throughflow is open. The artificial high-latitude meridional boundaries are impermeable, and the boundary conditions of zero meridional flux of temperature and salinity are imposed there. Poleward of the latitudinal limits of the ocean GCM, climatological values of the SST are used as boundary conditions for the AGCM. This specification includes sea ice extent. The SST produced by the OGCM and the climatological SST are blended smoothly over a 10° latitude zone near the artificial high latitude ocean meridional boundaries.

The ocean is initially at rest, with temperature and salinity set to climatological 1 January values from the data of Levitus (1982). Consequently, the ocean is spinning up during the initial phase of the coupled integration.

c. Coupling

To couple the two models, the solar radiation and surface fluxes of heat, salinity, and momentum at the ocean surface as simulated by the atmospheric model were updated for the ocean model once daily. The SST simulated by the ocean model for the same interval was then applied to the atmospheric model. The coupling fields were time averaged over the coupling interval. No runoff contribution was included in the calculation of the salinity flux into the ocean. The GFDL Modular Interface for Coupled Air–Sea Applications (MICASA) system (A. Rosati 1990, personal communication) was used to interpolate the coupling data between the AGCM and OGCM grids. The ocean model horizontal grid is much finer than the AGCM grid. The coupling scheme supplies the average ocean model SST over the area enclosed by the atmospheric grid box to the AGCM. The AGCM-produced fluxes supplied to the ocean model are linearly interpolated from the atmosphere to the ocean grid. The surface fluxes applied to the ocean model were those computed by the radiative transfer calculation and the bulk formulas of the atmospheric model; no empirical flux corrections to force the surface fluxes to conform to observations were applied. However, where possible the physical parameterizations were tuned to produce a more realistic simulation. A simplified 360-day astronomical year was adopted for the incoming solar radiation. Monthly (30-day) mean diagnostics were saved for analysis.

An empirical correction to the wind stress (Huang and Schneider 1995) was used in the final version of the coupled model (simulated years 46–62). At atmospheric grid points adjacent to coastlines in the tropical eastern Pacific and eastern Atlantic between the equator and 15°S, the wind stress used to force the ocean was taken as the average of the values at the three nearest atmospheric model grid points at the next longitude to the west (unless one of these was adjacent to the coast) rather than using the local value. The motivation for this correction came from uncoupled integrations of the ocean model described later in this section and initial results from the coupled model as described in section 2d.

The component models were subjected to separate verification tests. Two 13-yr integrations of the atmospheric model using observed SSTs from 1979–91 at the lower boundary were conducted. Similarly, multiyear integrations of the ocean model were done with observed wind stress forcing for the same period (Huang and Schneider 1995). Both models appear to be able to simulate many features of the annual cycle and interannual variability in the Tropics realistically. However, there are noticeable errors in both simulations. The atmospheric model intertropical convergence zone (ITCZ) in the eastern Pacific is diffuse compared to observations and tends to form in the Southern Hemisphere parallel to the equator in boreal spring, rather than remaining to the north of the equator as observed (Fig. 9). The ocean model appears to have a systematic cold bias in the eastern equatorial Pacific SST and the western equatorial Pacific heat content. Also, the eastern Pacific equatorial cold tongue simulated by the ocean model is too narrowly confined to the equator.

The potential impact of AGCM errors has been examined by forcing the ocean model with the wind stress produced by one of the observed SST 13-yr AGCM integrations (Huang and Schneider 1995). The ocean model response to wind stresses produced by the AGCM is realistic at the slower timescales. However, the mature El Niño equatorial SSTs are interrupted by cold anomalies in boreal spring, contrary to the observed evolution. The error may be related to the incorrect southward shift of the ITCZ in boreal spring in the uncoupled AGCM integrations. In the coupled case, in which the SST anomalies are coupled to evolution of the wind stress, this type of error could lead to inaccurate simulation of the characteristics of the interannual variability.

Near the coast of Peru, large positive SST errors were found from the ocean model forced by AGCM wind stress. This error was diagnosed as due to the tendency of the AGCM to produce winds that blow into the continent rather than along the shore as observed. The incorrect wind direction led to reduced coastal upwelling and SSTs that were too warm. When the wind stress near the coast between the equator and 15°S was taken from the AGCM one grid point (7.5° longitude) to the west, where the wind direction tends to be more parallel to the shore, the error was significantly reduced. However, this correction did not improve the simulation when applied north of the equator.

d. Experiments

The results to be described in the following sections are taken from the last 17 years of a 62-simulated-year integration of the coupled model. The model climate is close to equilibrium for this period. The model code was changed a number of times in the initial, spinup stages of the integration to improve the simulation of the mean climate and to eliminate coding errors. The chronology of those changes is described next. The statistics of the annual cycle and interannual variability actually change very little from years 25–63 of the integration. It was decided not to include the period when the model code was being upgraded in the analysis period for reasons of homogeneity.

The initial configuration of the coupled model was integrated for nine simulated years. During this period the coupled model experienced an unacceptably large climate drift. The global mean surface temperature was cooler by 0.5°C at the end of this period, and, more importantly, the SSTs in the tropical western Pacific were 3°C cooler than observed. The cooling showed no signs of abating. Additionally, unrealistic warming of

several degrees occurred equatorward of 30° latitude close to the eastern boundaries of the Pacific and Atlantic Oceans. The time-mean structure of the equatorial Pacific SST was severely distorted.

A diagnosis of the surface heat budget in the equatorial Pacific was done. The most unrealistic feature was that the shortwave radiation absorbed at the sea surface in the western tropical Pacific was smaller than observed by on the order of 50 W m^2, while the solar radiation absorbed at the sea surface in the eastern tropical Pacific was larger than observed by as much as 100 W m^2. Aspects of the parameterization of cloud–radiation interaction were determined to be the cause of these problems.

The western Pacific problem was caused by too much scattering of solar radiation by convective clouds. The Slingo-type (1987) scheme treats layer and convective clouds separately. The layer clouds are restricted to occupy only four of the model layers: one layer for high clouds, one for middle clouds, and two for low clouds. The original Slingo scheme allows only one low cloud level, but the COLA model layers, adopted from the original NMC model, are very thin near the ground, so very low clouds are specified to occupy two levels. These layer clouds are treated as uncorrelated in the vertical. Convective cloud towers are taken to occupy all levels between thermodynamic cloud base and cloud top, but with the understanding that cloud structures are highly vertically coherent. The cirrus cloud amounts associated with deep convection are determined empirically from the convective precipitation rate. The radiative code allows only randomly overlapped cloud layers in the vertical, which is appropriate only for the layer clouds. The choice had been made to treat the convective cloud towers inappropriately as randomly overlapped. Since they occur in all layers between cloud base and cloud top, which can be as much as 80% of the pressure depth of the atmosphere, even a small amount of supposedly convective cloud can have a large erroneous effect when treated as a thin haze. This inconsistency led to a large and incorrect reduction in the solar radiation reaching the surface in the convectively active tropical western Pacific.

Since the convective clouds could not be treated correctly by the radiation code, they were set to zero, pending improvement of the radiation code. This adjustment is included in the experiments described below. Convective cloudiness has also been the subject of tuning in at least one other coupled model (Stockdale et al. 1994). In our case, the procedure was expected to lead to errors of the opposite sign, with too much solar radiation reaching the ocean surface in the western tropical Pacific. However, we anticipated that the convective cloudiness, if correctly modeled, would be responsible for only a minor part of the cloud–radiation interaction in this region. The major contribution, certainly to the longwave radiation, should come from the cirrus, which are appropriately treated as layer clouds. However, it was discovered after the integrations described in this paper were completed that the computer code did not allow cirrus for pressures lower than 250 mb. The outcome is that the results reported below have erroneously large solar radiation reaching the surface and erroneously large longwave radiation leaving the top of the atmosphere in convectively active regions. These problems will be corrected in future studies.

The stratus cloud parameterization was examined because of the erroneously large solar flux reaching the ocean surface and the erroneously warm SSTs near the eastern boundaries of the tropical Pacific and Atlantic. Stockdale et al. (1994) also examined the sensitivity of their coupled model to the stratus. A coding error was found that prevented the stratus from forming. This error was corrected. Neither the convective cloud nor stratus problem is thought to have seriously impacted prior uncoupled studies with the COLA AGCM.

After these changes were made, the integration was restarted from conditions taken from the beginning of the fourth year of the original run. Counting simulated years from the initial conditions, the integration was continued out to 45 years. A coding error related to atmospheric mass conservation was corrected at the beginning of simulated year 16, and coding errors related to moisture conservation and surface wind stress (serendipitously repeating the error described in footnote 1 of Manabe and Bryan 1969), were corrected at the beginning of years 16 and 25. The simulation of the tropical SSTs improved markedly, with western Pacific SSTs recovering to near observed values. However, there was little reduction in the SST errors in the eastern Pacific and Atlantic. The solar radiation reaching the ocean surface in these regions was reduced by about 20 W m^{-2}, but the downward longwave radiation increased by almost the same amount. Since the stratus are low, warm clouds, the reduction in incoming solar radiation was nearly compensated by the increased longwave emission from cloud base. This nearly complete compensation is unrealistic, being prevented in reality by the large infrared optical thickness of the moist tropical boundary layer (D. Randall 1995, personal communication).

Despite the incorporation of the stratus cloud–radiation interaction and the correct model simulation of marine stratus in the observed locations near the coasts of Peru and Africa, the erroneously warm SSTs persisted at these locations. Therefore, the wind stress extrapolation procedure described above was implemented in the coupled model beginning in year 46 of the integration. It was hoped that improving SST near the coast would lead to improvement away from the coast by advection. There was some improvement of the SST in the regions in question; however, this was restricted to locations very near the coastline. The model with the coastal correction produced annual mean SST 7°C cooler near between 5° and 10°S at the west coast of South America and 6°C cooler near between 5° and 10°S at

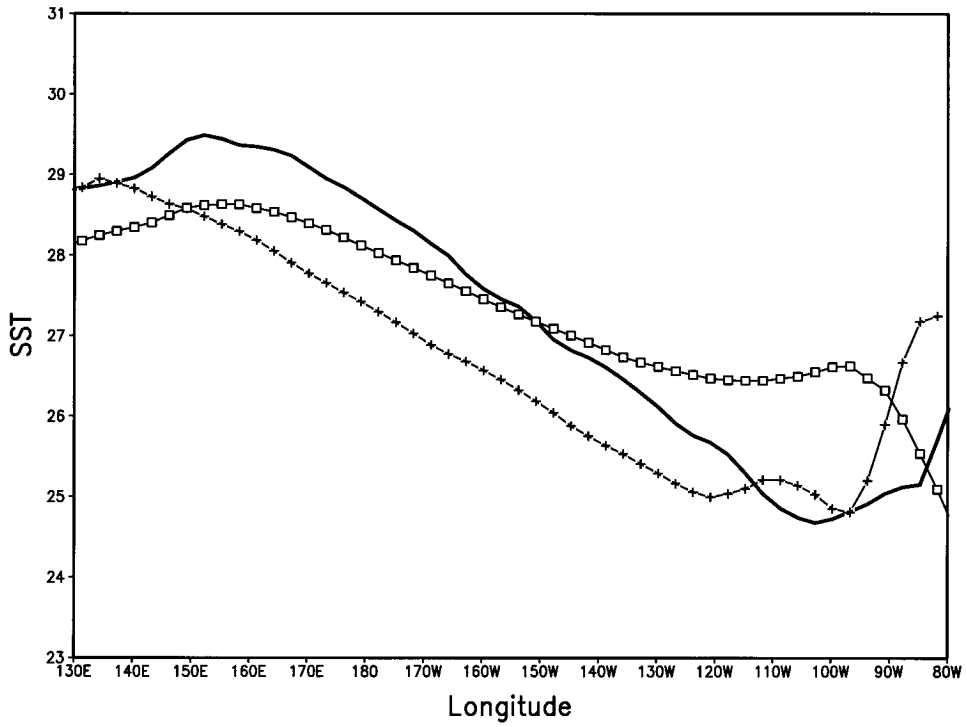

FIG. 1. Annual mean SST (°C) at the equator: (a) observed (thick solid curve) from 1978–87 COADS data (as processed by the Climate Analysis Center), (b) diagnosed from the ocean model output (crosses), (c) diagnosed from the atmospheric model output (open squares).

the west coast of Africa. The effect of the correction decayed to zero within a few degrees to the east in the Pacific. Behavior in the Atlantic was similar, but additionally there was also a noticeable strengthening of the equatorial cold tongue. The model adjusted quickly to the wind stress correction, and the model climate remained close to equilibrium for years 46–62 of the integration. The analysis presented below is restricted to results from this time period.

3. Results

The coupled model climate drift appeared to be small during the final 17 years, 46–62, of the simulation. The linear trend in the global mean surface temperature in this period is estimated to be a warming of about 0.006 K yr^{-1}. The final 17-yr period was chosen for analysis of the annual mean, annual cycle, and interannual variability in the tropical Pacific, as well as examination of the relationship between the interannual variability of tropical Pacific SST and the global atmosphere. The model climatology is compared with various analyses of the tropical Pacific Ocean climatology, including Levitus (1982), Ji et al. (1995, referred to as the NMC analysis), and one based on COADS (Comprehensive Ocean–Atmosphere Data Set). These analyses have their own associated problems, which are not the subject of this report and will not be discussed further, but we believe that the errors in the simulation that will be emphasized are large compared with the errors in the analyses.

a. Annual mean

Figure 1 shows SST at the equator as obtained from the ocean model output, as interpolated to the atmospheric grid, and COADS. The ocean model maintains the east–west temperature gradient at the equator at slightly less than observed values but is about 1°C cooler than observed over most of the central and western Pacific. The ocean model results are about 0.3°C warmer than those showxn for the COLA coupled model (years 16–25 of this integration) in Mechoso et al. (1995, Fig. 1). However, the ocean SST grid point nearest the eastern boundary is 1.5°C cooler than found in the earlier results, with the difference due to the empirical wind stress interpolation. This cooling does not extend away from the coast of Peru.

The equatorial Pacific SST as seen by the AGCM is also shown in Fig. 1. It has much weaker east–west gradients than the ocean-grid SST. Even the sign of the gradient is different near the eastern boundary. This difference, away from the eastern boundary, results from the combined effect of two inaccuracies. First, because the atmospheric model grid meridional resolution (4.5° latitude) is coarse relative to the ocean model meridional resolution (0.5° latitude) near the equator, the coupling scheme supplies the atmospheric model with a highly

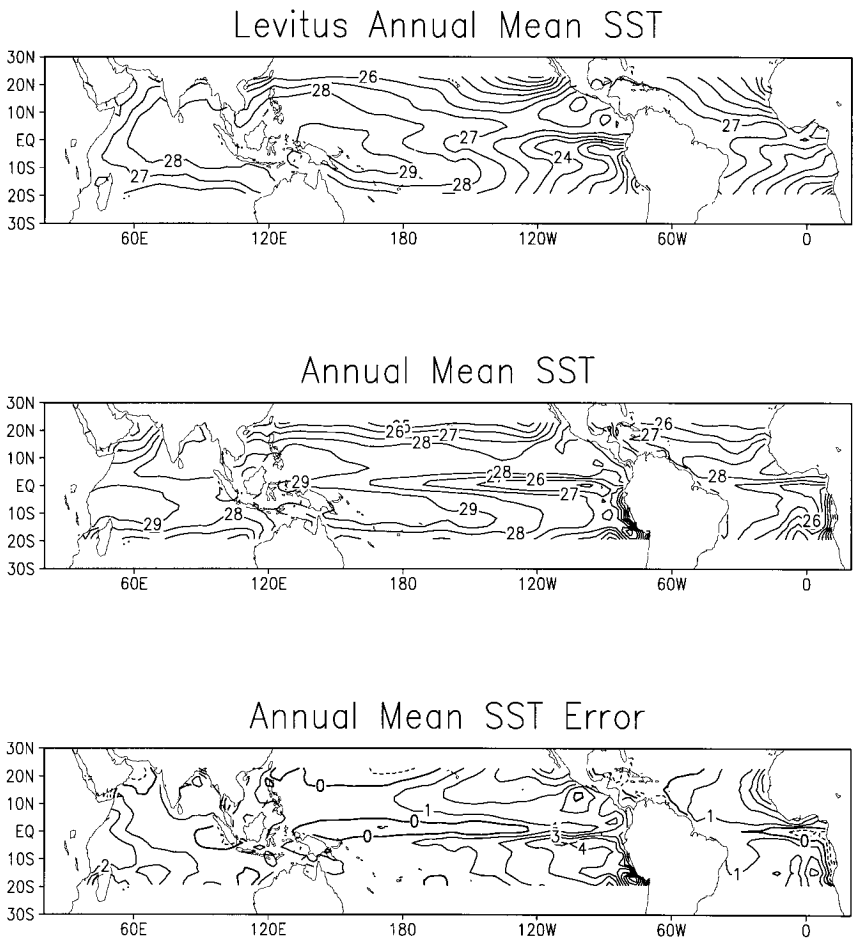

FIG. 2. Annual mean SST (°C). Top: observed (Levitus 1982). Middle: coupled model integration averaged over years 53–62. Bottom: error in coupled model integration. Contour interval 1°C.

meridionally smoothed version of the SST calculated in the ocean model. Second, the ocean model systematically produces an erroneously narrow equatorial cold tongue, even with the observed wind stress forcing, as discussed above, so that the cold SSTs in the eastern equatorial Pacific are confined much too close to the equator. These two inaccuracies combine to lead to substantial weakening of the equatorial cold tongue in interpolation of the ocean model SST to the atmospheric grid. The local feedback between SSTs and wind stress close to the eastern boundary is of course totally misrepresented.

These problems could have serious consequences for the simulation of a realistic annual cycle and realistic ENSO variability. The delayed oscillator mechanism requires sufficiently strong coupling between equatorial SST anomalies and equatorial zonal wind stress. The weakening of the equatorial Pacific SST gradients as seen by the AGCM due to insufficient meridional resolution in the atmospheric model will effectively weaken the coupling between equatorial SST and the atmosphere. The erroneous narrowness of the cold tongue in the ocean model is an important contributor to this problem.

The annual mean SST taken from the ocean model for model years 53–62 is compared to the Levitus (1982) analysis in Fig. 2. The decadal period was used here for calculation of the climatology of some of the ocean model output for convenient comparison with the results from the prior decade of the integration shown in Mechoso et al. (1995). The ocean model climatology for years 46–62 is very similar to that from years 53–62. The coupled model eastern Pacific equatorial cold tongue is erroneously narrow, as expected from the uncoupled ocean model integration and as shown compared to COADS data for model years 16–25 in Mechoso et al. (1995, Figs. 3 and 4). Differences between the simulated SST and the Levitus (1982) analysis are less than 1°C over the Pacific west of the dateline. The model produces SSTs that are too warm by several degrees in the eastern Pacific. In contrast, the eastern equatorial Atlantic is cold compared to the Levitus (1982)

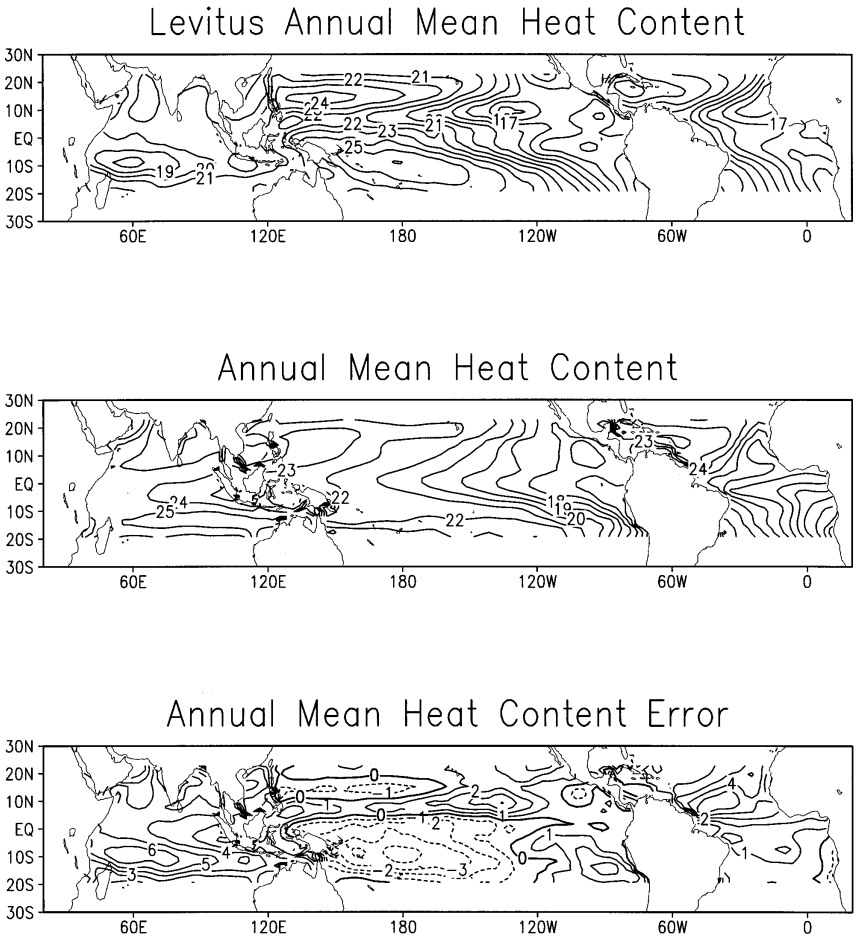

FIG. 3. Annual mean heat content defined as temperature (°C) averaged over top 232 m of the ocean. Top: observed (Levitus 1982). Middle: coupled model integration averaged over years 53–62. Bottom: error in coupled model integration. Contour interval 1°C.

analysis. The difference in the sign of the difference from the Levitus (1982) analysis in the equatorial eastern Atlantic and eastern Pacific results from a stronger equatorial sensitivity in the Atlantic than the Pacific to the empirical wind stress interpolation. The annual mean SST errors are less than 2°C over most of the tropical Atlantic and Indian Oceans. The root mean squared (rms) error of annual mean SST over the oceans equatorward of 20° latitude is 1.7°C.

The annual mean subsurface thermal structure is summarized by the heat content, defined here to be the temperature vertically averaged over the top 232 m, shown in Fig. 3. The coupled model fails to capture much of the structure of the heat content in the western Pacific and has large negative differences from the Levitus (1982) analysis there, except near 9°N, where the differences are positive. The gradients of heat content in the Southern Hemisphere Pacific are not well simulated. The simulation of the Pacific north of the equator is somewhat better. The general structure of heat content in the Atlantic is captured by the coupled model, although there are large positive errors near 10°N. The major feature in the Indian Ocean analysis, a maximum near 10°S and 60°E, is not simulated by the coupled model. The annual mean heat content simulated by Philander et al. (1992) is closer to the analysis than that obtained here.

Examination of the subsurface temperature (Figs. 4 and 5) verifies that the heat content differences reflect differences in the depth of the thermocline. The model thermocline is, if anything, sharper than that in the Levitus (1982) data. The 20°C isotherm appears to always lie in the region of strong vertical temperature gradients and will be taken as a measure of the thermocline depth. The thermocline depth in the equatorial western Pacific is about 50 m shallower than in the analysis, while the depth in the eastern Pacific is close to the analysis (Fig. 4). The east–west thermocline slope in the equatorial Pacific is only about 60% of the magnitude in the analysis, which indicates that the equatorial Pacific zonal wind stress is only 60% of the observed strength since these two quantities are directly proportional at the

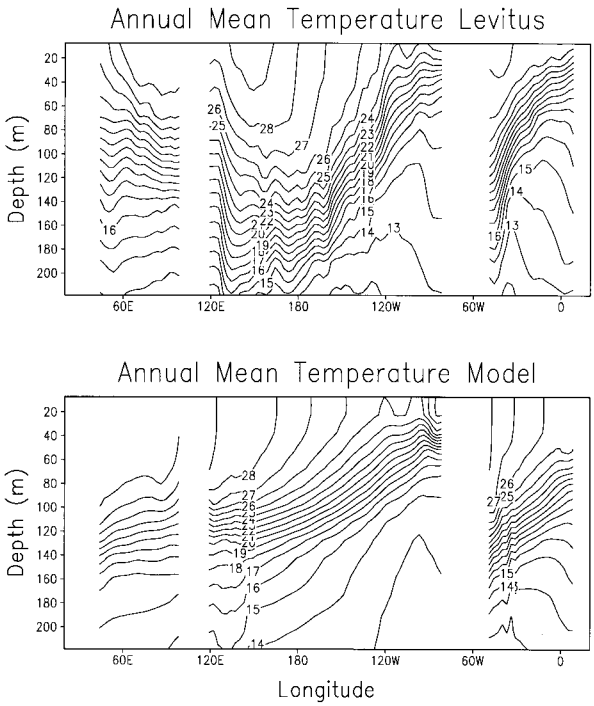

FIG. 4. Annual mean temperature (°C) in the upper ocean at the equator as a function of depth. Top: observed (Levitus 1982). Bottom: coupled model integration averaged over years 53–62. Contour interval 1°C.

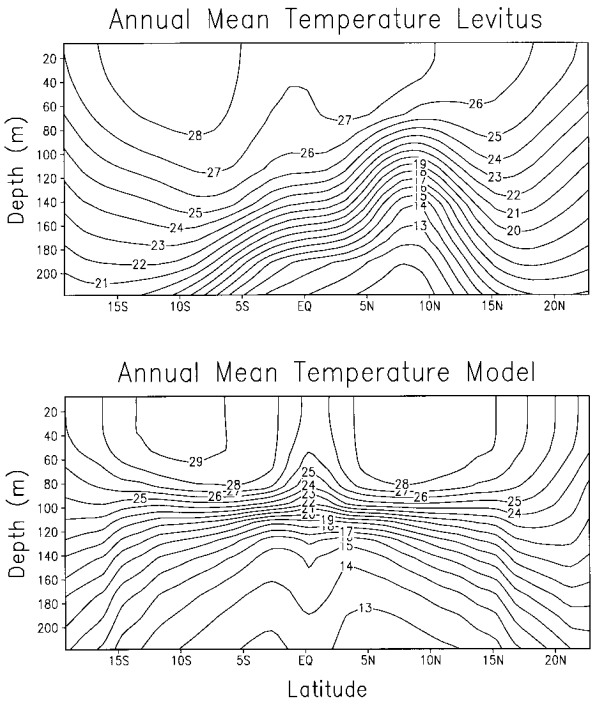

FIG. 5. Annual mean temperature (°C) in the upper ocean at longitude 165°W as a function of depth. Top: observed (Levitus 1982). Bottom: coupled model integration averaged over years 53–62. Contour interval 1°C.

equator on interannual timescales (Schneider et al. 1995). Errors in the simulation of the Atlantic and Indian Oceans are also evident in Fig. 4. The erroneous sign of the east–west slope of the isotherms in the upper 120 m of the Indian Ocean may point to problems in the zonal wind stress in that region. In the north–south section at 165°W (Fig. 5), the model Pacific thermocline depth is close to the observed depth at 10°N but is 100 m shallower than observed at 10°S. An error of similar magnitude but opposite sign is found in the Indian Ocean thermocline depth south of the equator.

Figure 5 shows that the model thermocline depth has practically no north–south slope and that the ocean temperature is nearly symmetric about the equator. The thermocline depth in the analysis, on the other hand, is highly asymmetric about the equator, with a marked deepening from the Northern to the Southern Hemisphere. Additionally, the model thermocline between 10°S and 10°N appears to be much sharper than in the analysis.

Annual mean surface currents in the Pacific for the coupled model and the NMC analysis for the period 1982–93 (Ji et al. 1995) are compared in Fig. 6. We caution the reader that this analysis resulted from assimilation of ocean temperature but not current measurements. The coupled model has stronger than analyzed eastward surface currents near the equator and much weaker currents off the equator. The North Equatorial Countercurrent is absent in the coupled model. The ocean model forced by wind stress derived from the Florida State University (FSU) pseudostress (Goldenberg and O'Brien 1981) produces a North Equatorial Countercurrent (Huang and Schneider 1995), so the absence of this feature in the coupled simulation is due to erroneous wind stress forcing from the AGCM.

The climatological subsurface structure simulated at the equator has also been compared to measurements taken from moorings (McPhaden and McCarty 1992; McCarty and McPhaden 1993). The errors in the simulated subsurface temperature are consistent with the differences between the simulation and the Levitus (1982) analysis. The simulated thermocline depth is erroneously shallow at 165°E and 140°W, and close to observed at 110°W. The strength of the simulated equatorial undercurrent is about half of the observed at 110°W and 140°W, and close to the observed value at 165°E. As with the thermocline depth, the depth of the simulated undercurrent is too shallow at 165°E and 140°W, and close to observed at 110°W.

The annual-mean atmospheric model climatology is shown in Fig. 7. The sea level pressure, precipitation, and wind stress fields appear realistic in many respects. The results in Fig. 7 are similar to those presented by Lau et al. (1992, Fig. 1) and their discussion applies. The major defects in the tropical Pacific appear to be a diffuse tropical precipitation field and weak wind stress. These defects are similar to those seen in the coarse horizontal resolution AGCMs that have been used in most long coupled simulations.

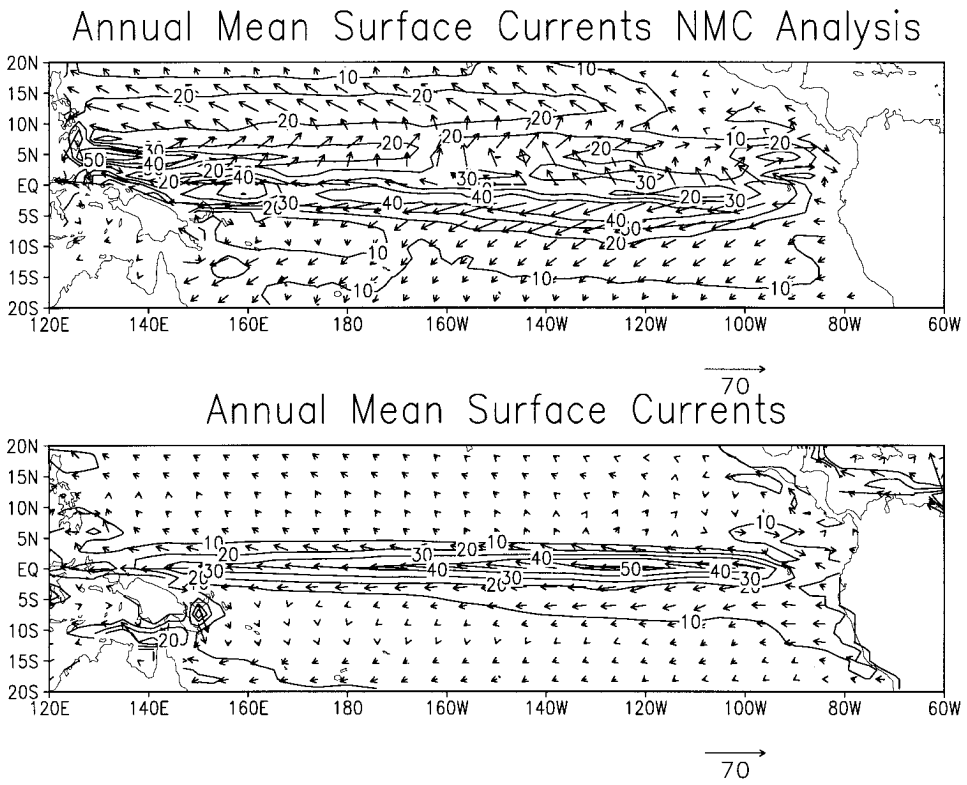

FIG. 6. Annual mean surface currents in the ocean. Top: NMC analysis (Ji et al. 1995). Bottom: coupled model integration averaged over years 53–62. The arrows in the lower right corners of the panels give the scale of the vectors (cm s^{-1}), and the contours give the magnitude with contour interval 10 cm s^{-1}.

b. Annual cycle in the tropical Pacific

The observed and modeled annual cycles of SST at the equator in the Pacific are compared in Fig. 8. The results are similar to those shown by Mechoso et al. (1995, Fig. 2) for years 16–25 of this coupled simulation. The structure of the model annual cycle is similar to that found in the observations. In both, maximum variations are found in the eastern Pacific and there is westward propagation. The phase of the model annual cycle is close to the observed over most longitudes. The maximum magnitudes are found somewhat farther from the eastern boundary and are somewhat weaker in the model than in the observations. The simulation for years 53–62 is better than the simulation for years 16–25 shown in Mechoso et al. (1995, Fig. 2) in that the behavior near the eastern boundary is slightly improved. This improvement is probably due to the empirical wind stress extrapolation in that region. The realism of the model annual cycle shown in Fig. 8 compares favorably with that from any of the other models shown in Mechoso et al. (1995, Fig. 2).

We have found that simulation of the annual cycle is sensitive to either resolution or physical parameterization changes that have been made in our model. An earlier version of the coupled model (Schneider and Kinter 1994) incorrectly produced an annual cycle with a strong semiannual SST variation in the equatorial eastern Pacific. The major differences between that simulation and the one described here are that in the previous work the ocean model resolution was somewhat lower, $3° \times 3°$ in the horizontal and 13 levels in the vertical; the atmospheric model had only nine levels in the vertical; and that penetration of solar radiation was not included in the previous work. The cause of this sensitivity is currently being isolated.

Seasonal mean maps of tropical precipitation are shown for 1979–93 observations (Ropelewski et al. 1985; Spencer 1993) in Fig. 9 and for model simulation over years 46–62 in Fig. 10. The major problems over the Pacific are the absence (December–February, March–May) or diffuseness (June–August, September–November) of the ITCZ, located parallel to and to the north of the equator. The South Pacific convergence zone (SPCZ) in the model tends to be too zonally oriented. The model described by Nagai et al. (1992, Fig. 4) produces a better representation of the ITCZ than this coarse horizontal resolution version of the COLA model.

c. The model ENSO

The characteristics of the model ENSO are discussed in this subsection. Time series of the unfiltered monthly

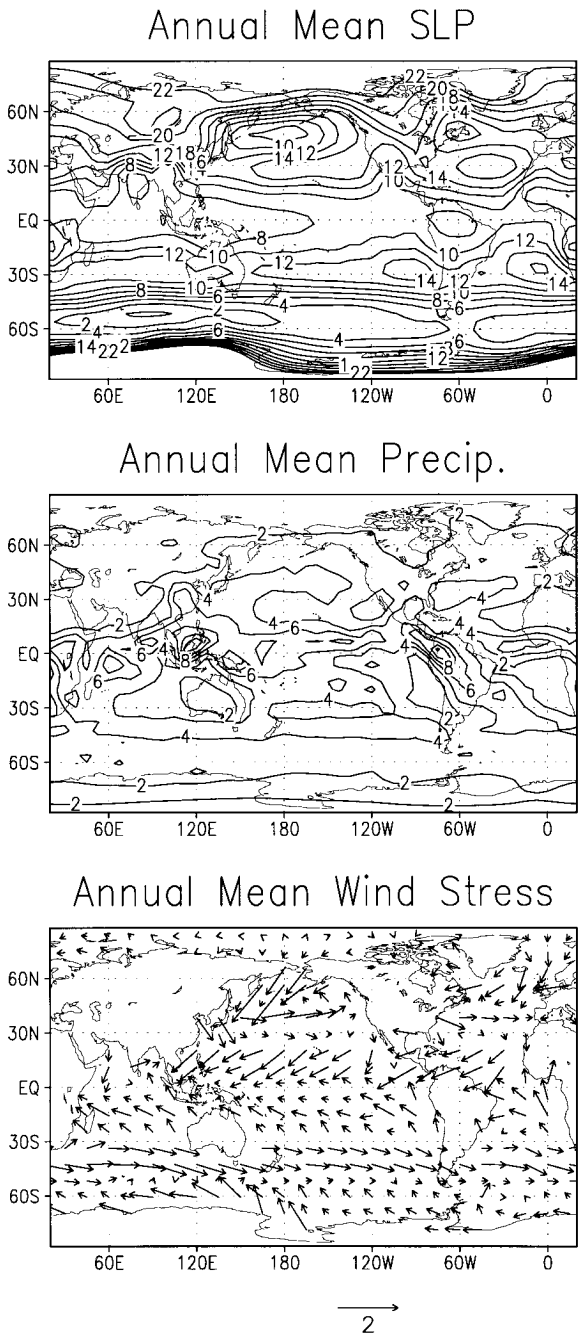

FIG. 7. Annual mean surface fields from the coupled run, years 46–62. Top: sea level pressure (mb − 1000). Middle: precipitation (mm day^{-1}). Bottom: wind stress on the ocean (dyn cm^{-2}) with scale given by the arrow at the below of the panel.

mean data in the tropical Pacific show features characteristic of the delayed oscillator mechanism (Schopf and Suarez 1988; Battisti and Hirst 1989). An extended empirical orthogonal function (EEOF) analysis of the tropical Pacific anomalies shows an evolution of SST and heat content similar to that one found using the same OGCM forced by observed wind stress (Huang and Schneider 1995). Finally, correlation analyses are used to examine the global scale aspects of the model ENSO.

1) SST AND HEAT CONTENT TIME SERIES

Figure 11 shows the coupled model equatorial SST anomalies from the annual cycle for years 46–62, as produced by the ocean model. The SST anomalies have maximum magnitudes in the central and eastern Pacific. Interannual variability of SST is irregular. Coherent warm events of significant magnitude occur in years 48, 51, and 62 and cold events occur in years 47, 49–50, and 59. An extended period of small interannual variability occurs from years 52–58. An estimate of the period is (17 yr)/(3 full cycles) ≈6 yr. Since there is a 7-yr quiescent period in the middle of the integrations, another estimate of the period (active phases only) is about three years. The SST events last somewhat less than a year. They are phase locked to the annual cycle, terminating in boreal spring. The typical event has maximum amplitude SST anomalies of about 1°C. The SST anomalies at the equator do not exhibit systematic propagation. The concentration in the eastern and central Pacific, the irregular interannual variability, the 3–6-yr period, and the lack of systematic propagation are similar to the behavior of observed events, but the amplitude is only about half that of observed equatorial SST anomalies.

Some interannual equatorial SST variability was simulated in the Atlantic and Indian Oceans, as can be seen in Fig. 11, but was much weaker than and uncorrelated with that in the Pacific. Interannual variability of equatorial SST with a similar character to that shown in Fig. 11 was found throughout the 62 years of the integration.

The heat content anomalies from the year 46–62 climatology at 5°S, the equator, and 5°N are shown in Fig. 12 for the last 17 years of the integration. Zonal wind stress anomalies at the equator are superposed. Some characteristic features of the delayed oscillator mechanism (Schopf and Suarez 1988; Suarez and Schopf 1988; Battisti and Hirst 1989) can be seen in this figure. Heat content anomalies propagate predominantly eastward at the equator and westward at 5°S and 5°N. On the interseasonal timescale, wind stress events at the equator appear to simultaneously force eastward propagating Kelvin waves of the same sign (i.e., positive heat content anomalies forced by positive wind stress anomalies) at the equator and more slowly westward propagating Rossby waves of opposite sign more or less symmetrically about the equator. The eastward propagation at the equator is modulated by a more slowly propagating envelope that takes about a year to cross the basin. The time lag for the westward propagating signals at 5°N between the dateline and the western boundary is about 4 months. The waves amplify and decay in a manner consistent with their being modified by the wind stress along their characteristic trajectories.

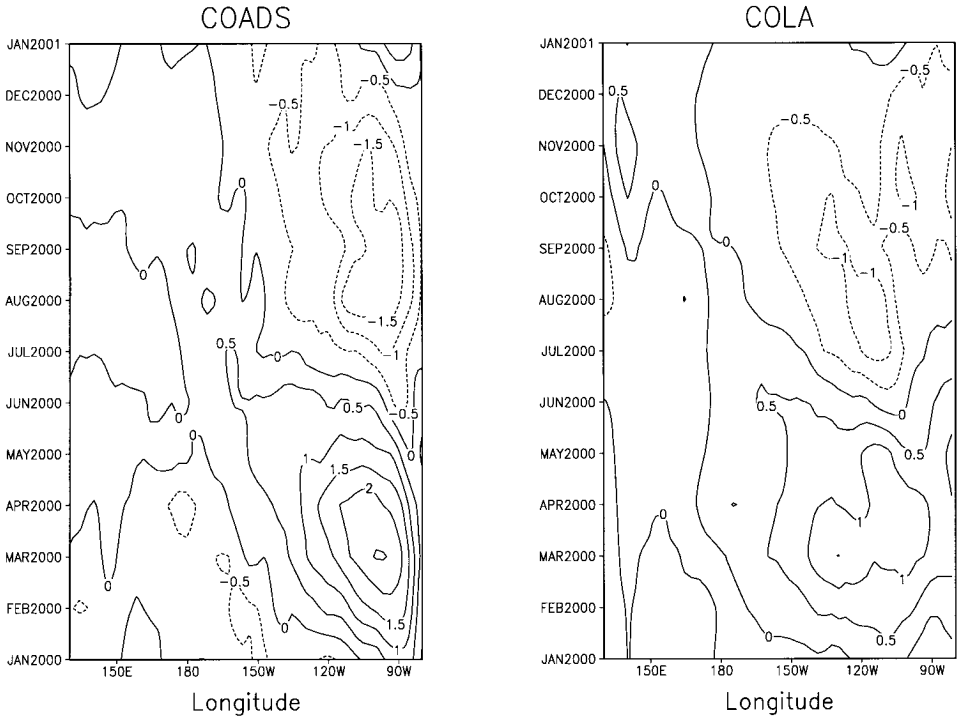

FIG. 8. Annual cycle of SST (°C) at the equator, annual mean removed. Left: observed (1978–87 COADS data as processed by the Climate Analysis Center). Right: coupled model, years 53–62. Contour interval 0.5°C.

The Rossby waves that reach the western boundary appear to reflect as Kelvin waves. The largest heat content anomalies in the eastern Pacific are associated with the largest warm and cold events shown in Fig. 11.

However, there are several significant differences between the behavior shown in Fig. 12 and that diagnosed for 1986–92 in Schneider et al. (1995). The amplitudes of heat content and wind stress anomalies are only about half of the observed values. The wind stress anomalies in the coupled simulation are less coherent spatially and temporally. Observed wind stress anomalies are more concentrated in the central Pacific. Relative to anomalies in the central Pacific, coupled model simulated wind stress anomalies in the far western and far eastern Pacific are much larger than observed. The speed of eastward propagation of the heat content envelope at the equator in the western Pacific is faster than observed. The magnitudes of heat content anomalies in the western Pacific are smaller relative to anomalies in the eastern Pacific than observed both on and off the equator.

Consideration of the simple time delay model given in Schneider et al. (1995) shows that the reduced amplitude of the heat content anomalies at the western boundary at the equator relative to the eastern boundary indicates a smaller influence of Rossby waves near the equator than in the real climate system. This conceptual model has two components: 1) an east–west equatorial thermocline slope in equilibrium with the equatorial wind stress anomalies and 2) heat content anomalies at the western boundary produced by westward propagating Rossby waves forced by prior wind stress anomalies. One important forcing for Rossby waves in the equatorial waveguide is the curl of the wind stress anomalies (Chao and Philander 1993). Since the coarse horizontal resolution AGCM does not resolve the meridional variations of the wind stress well, the Rossby wave forcing could be underestimated, leading to weak heat content anomalies at the western boundary. It is also possible that the longitudinal structure of the wind stress anomalies produced by the AGCM is erroneously configured so as to lead to more destructive interference along Rossby wave characteristics than observed wind stress anomalies (Schneider et al. 1995). The reduction of the Rossby wave forcing should reduce the instability of the coupled system [Schneider et al. 1995, Eq. (7)] but will not affect the period of the oscillations directly. The period will depend on the spatial structure of the wind stress forcing.

2) EEOF ANALYSIS

The typical evolution of the SST, heat content, and zonal wind stress on interannual timescales in the tropical Pacific was found by an extended empirical orthogonal function analysis (Weare and Nasstrom 1982). A similar analysis for the ocean model forced by wind stress constructed from the FSU pseudostress, which we will refer to as the observed wind stress, from 1979 to

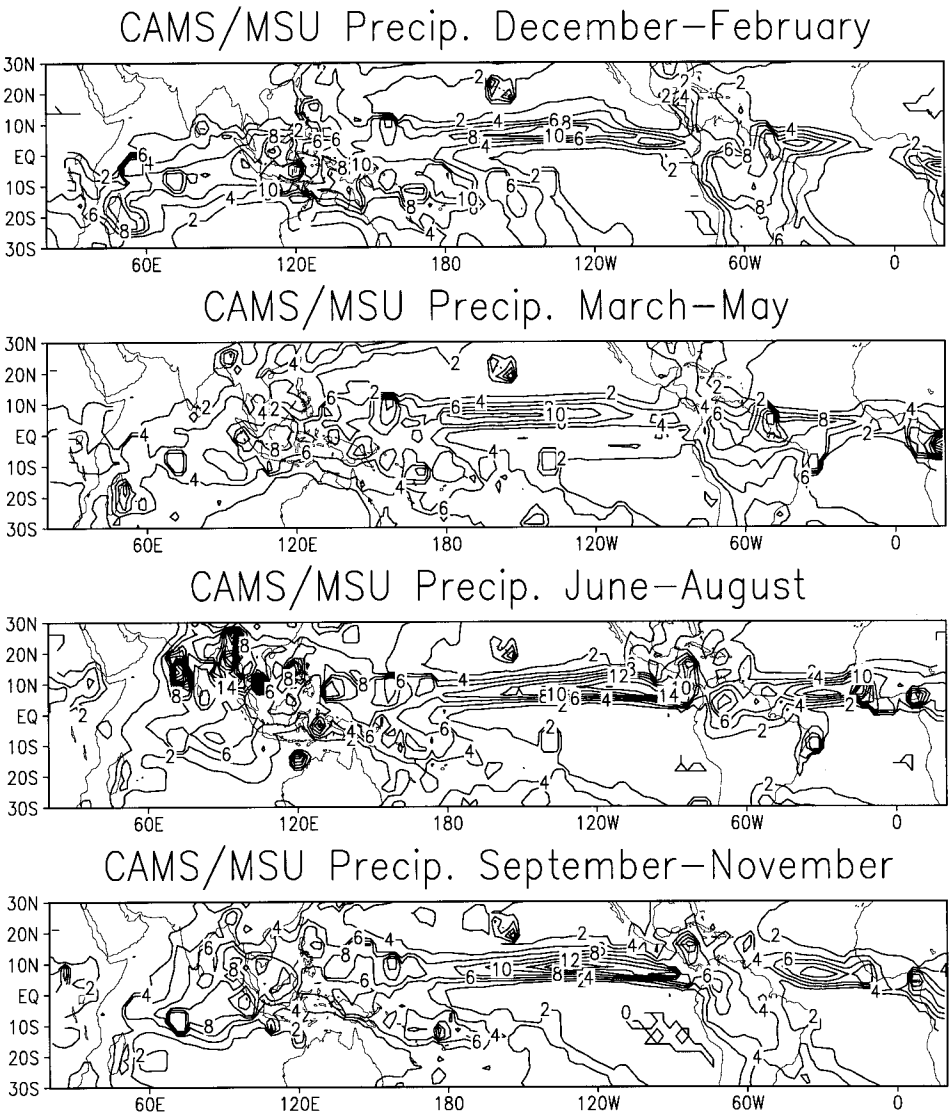

FIG. 9. Annual cycle of 1979–93 observed low-latitude precipitation (Ropelewski et al. 1985; Spencer 1993). Time periods are indicated at the top of each panel. Contour interval 2 mm day^{-1}.

1991 was made by Huang and Schneider (1995). The length of the window used to construct the EEOFs here was 16 seasons. The leading two patterns, which represent the same evolution starting from different phases, together account for 20% of the variance. The interannual evolution at the equator (Fig. 13) has the characteristics described above: a standing oscillation in SST with maximum amplitude in the eastern Pacific, eastward propagating heat content anomalies with maximum amplitude also in the eastern Pacific, and maximum SST anomalies coinciding in time with arrival of the heat content anomalies in the eastern Pacific. The zonal wind stress has maximum amplitude in the central Pacific and western Pacific. We have verified that pressure gradients due to the east–west slope of the thermocline are in balance with the wind stress at the equator. The wind stress in the central Pacific is in phase with the SST anomalies in the central and eastern Pacific. The wind stress displays slow westward propagation in the western Pacific, as does the SST. The structure of all three fields in the western Pacific is unrealistic. The amplitude of the heat content anomalies is too small there, and westward propagation of wind stress and SST is not observed. Apparently, the coupling between wind stress and SST is too strong there and the subsurface response too small.

The heat content from the EEOF analysis at 5°S and 5°N is shown in Fig. 14. There is westward propagation in the EEOF analysis in the western Pacific at 5°N. The phase speed of this propagation appears to be slower than is apparent off the equator in Fig. 12. There is no obvious westward propagating signal at 5°S, contrary

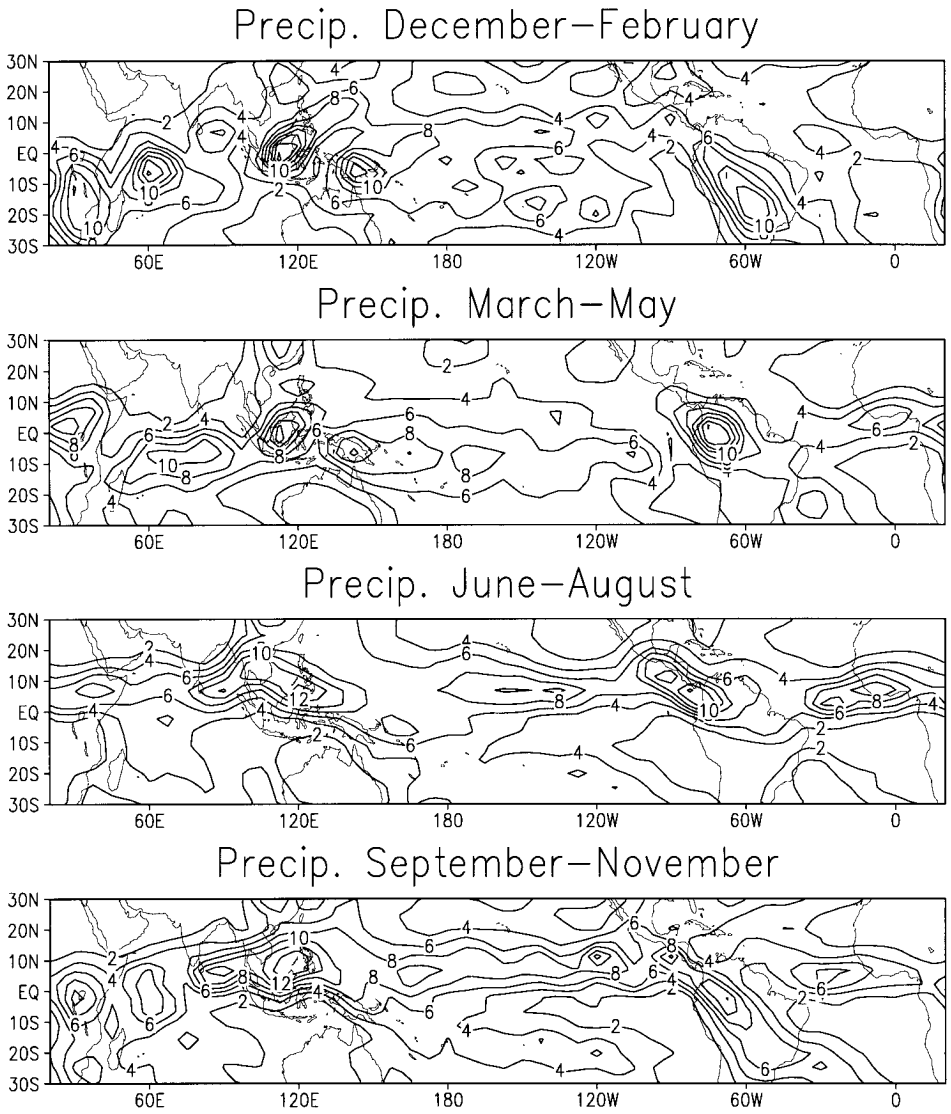

FIG. 10. Annual cycle of low-latitude precipitation from model simulation, years 46–62. Time periods are indicated at the top of each panel. Contour interval 2 mm day^{-1}.

to what might be expected from examination of Fig. 12. In the central Pacific, the direction of propagation is eastward, and the pattern appears to be associated with the eastward propagating heat content anomaly at the equator. The heat content evolution in the central and western Pacific is not symmetrical about the equator except near the western boundary. Comparison with the wind stress in Fig. 13 suggests that the slow westward propagation at 5°N is associated with the westward propagation of the equatorial wind stress anomalies.

The results of the EEOF analyses of the coupled model described here and the one of the OGCM forced by the observed wind stress (Huang and Schneider 1995, Fig. 12) are similar in many respects. The spatial structure of, and relationship between, the SST and heat content anomalies follows basically the same sequence in both instances. Primarily nonpropagating SST anomalies are found in both cases. Eastward propagating heat content anomalies are prominent at the equator. The asymmetrical structure of the heat content evolution about the equator discussed above, with westward propagation found primarily in the Northern Hemisphere, is also found in the dominant EEOFs of the simulation with observed forcing. There are, however, some major differences. The coupled model has largest amplitude in SST anomalies in the far eastern equatorial Pacific, while the simulation with observed wind stress forcing produces maximum amplitude in the central equatorial Pacific. The coupled simulation is more realistic in this respect. The coupled model never develops a tropically confined pool of anomalous high/

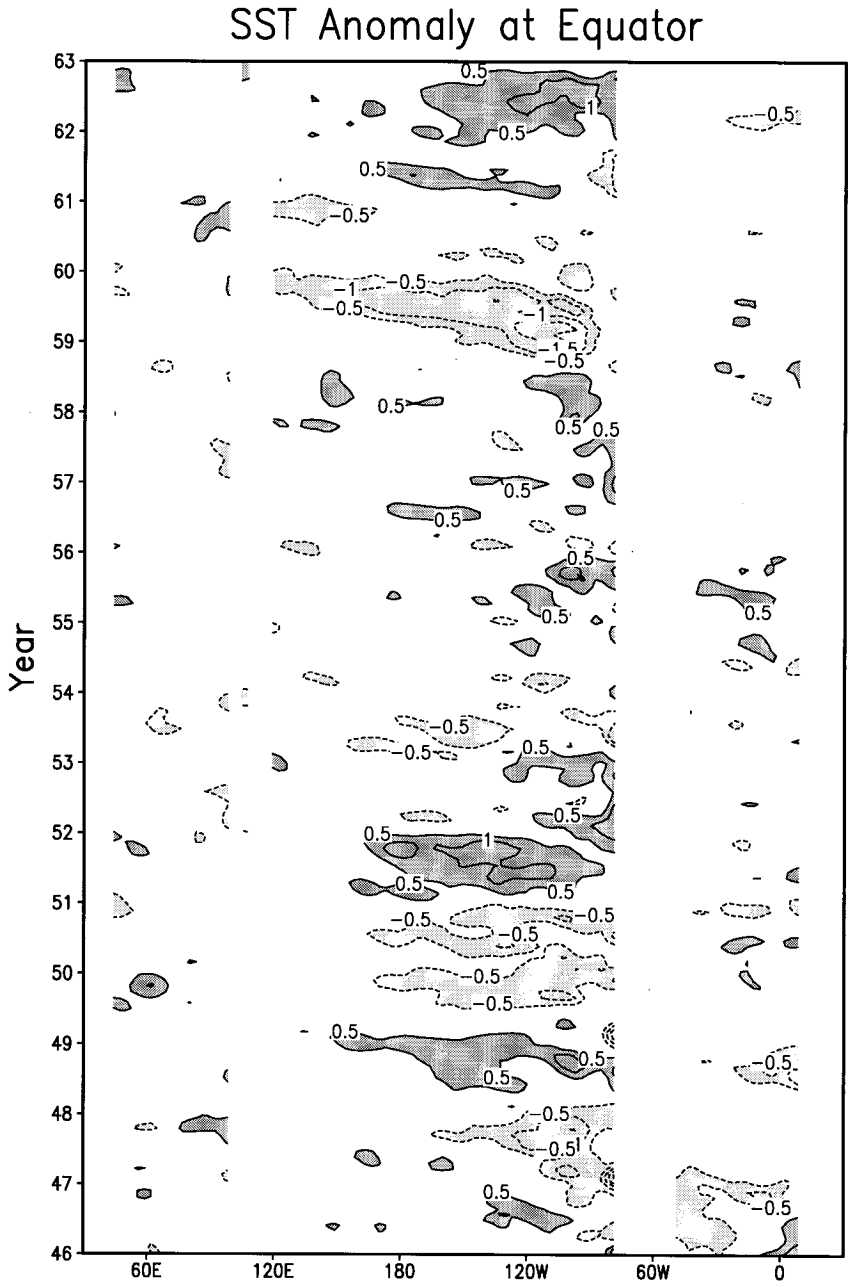

FIG. 11. Equatorial SST anomalies from the annual cycle in the coupled model integration. Contour interval 0.5°C, zero contour suppressed. The vertical axis is year of integration.

low heat content in the western Pacific such as the one that occurs in the forced simulation as a major precursor of a warm/cold SST event (Huang and Schneider 1995, Fig. 12h).

The EEOF analysis suggests a weakened and distorted delayed oscillator mechanism for the model's interannual equatorial Pacific SST anomalies. The Rossby wave link in the western Pacific of the coupled simulation, which produces the heat content anomalies near the western boundary, is weak. Possible reasons for this deficiency have been discussed above.

3) GLOBAL-SCALE ASSOCIATIONS

Finally, we briefly examine features associated with the simulated equatorial Pacific SST anomalies, concentrating on the global scales. A singular-value decomposition (SVD) analysis (Bretherton et al. 1992) of the November–January (NDJ) SST anomalies over the tropical Pacific and 200-mb height anomalies was carried out for years 46–62. The NDJ season was chosen rather than the more conventional December–February period because the simulated SST anomalies in the east-

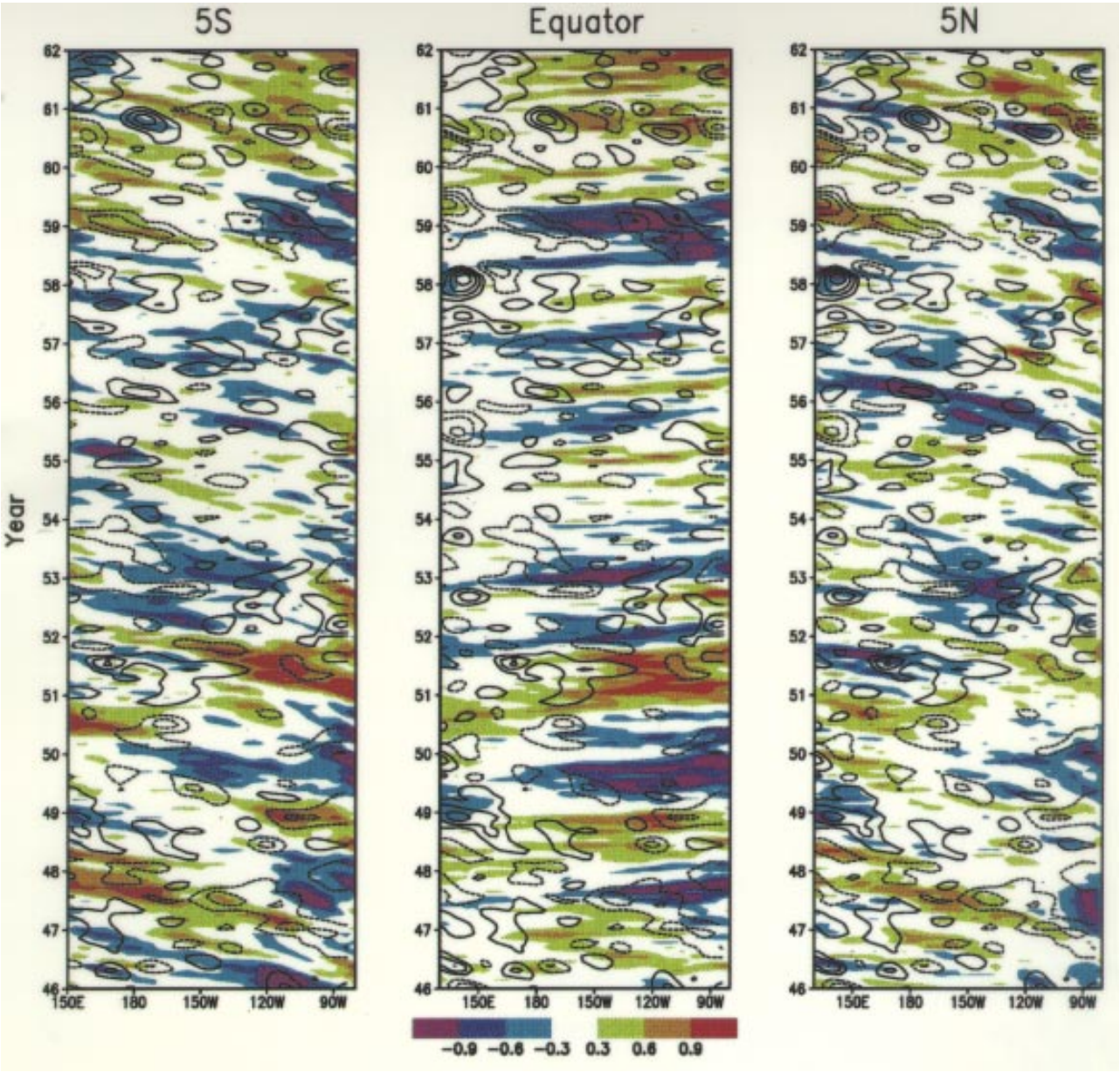

FIG. 12. Heat content (vertically averaged temperature) anomalies (°C) in the tropical Pacific (shaded) from the last 17 years of the coupled model simulation. Left: 5°S. Center: equator. Right: 5°N. Contours are equatorial zonal wind stress anomalies, contour interval 0.05 dyn cm^{-2}, zero contour suppressed. The wind stress anomalies have been subjected to two passes of a nine-point space–time smoother. The vertical axis is year of integration.

ern Pacific are phase locked to the annual cycle and become small in February. The SST and geopotential patterns and the time series for the first mode, which explains 65% of the cumulative squared covariance, is shown in Fig. 15. The SST pattern is close to that found in the mature event phase of the EEOF discussed above and will be taken to represent the mature event structure. There is a coherent nearly zonal response in the tropical and subtropical 200-mb geopotential, which corresponds to a general warming of the low-latitude troposphere. The zonal uniformity of the low-latitude atmospheric 200-mb geopotential response to localized heating anomalies can be understood as due to the inefficiency of the Coriolis effect in compensating for pressure gradients in low latitudes and the nearly inviscid character of the time-mean upper-tropospheric motions there (Schneider 1987). The divergent response to convective heating then configures itself within the Tropics so as to remove the pressure gradients. The coupled model tropical atmosphere warms during a sim-

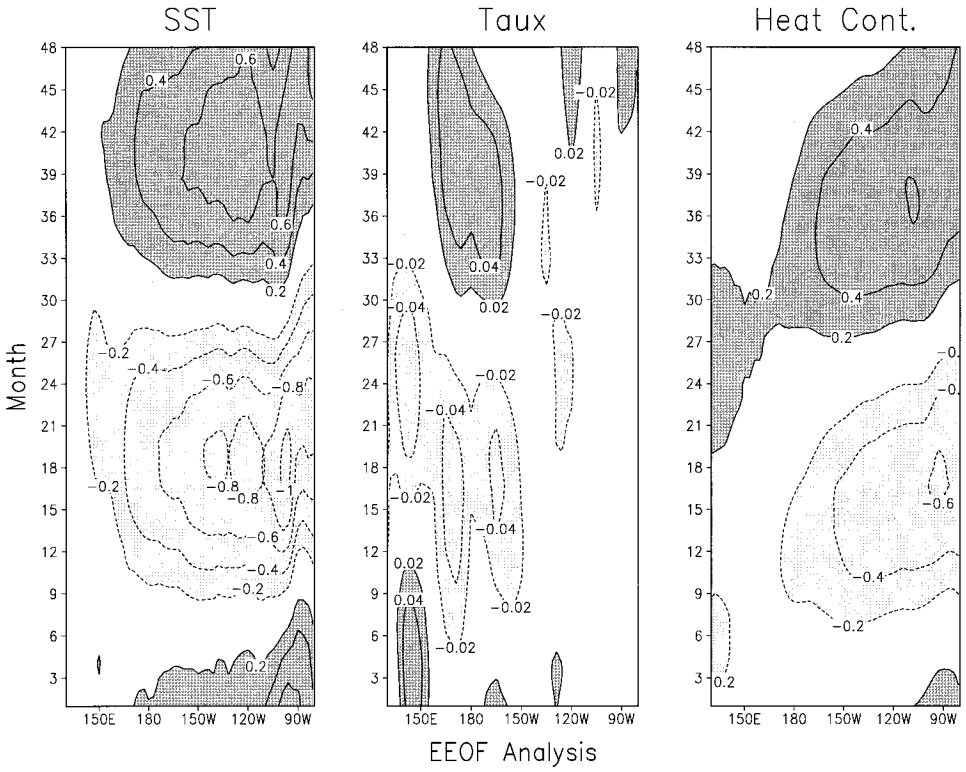

FIG. 13. Leading evolution pattern at the equator resulting from an extended empirical orthogonal function analysis with a 16-season window of the time series of SST, zonal wind stress, and heat content anomalies in the tropical Pacific. Left: SST (°C), contour interval 0.2°C. Center: zonal wind stress (dyn cm^{-2}), contour interval 0.02 dyn cm^{-2}. Right: heat content (°C), contour interval 0.2°C. Dashed contours denote negative values. The vertical axis is time in months.

ulated El Niño, as observed. The warming is due to a positive tropical zonal mean heating anomaly, which also forces a stronger Hadley circulation and a stronger and equatorward displaced subtropical jet stream (Schneider 1984). The strengthening and equatorward displacement of the simulated subtropical jet stream can be inferred from the 200-mb geopotential in Fig. 15.

There is also a modest amplitude midlatitude response to the tropical ENSO in the model. The Southern Hemisphere response is more zonally symmetric that the Northern Hemisphere response. There appears to be little preference for any particular longitude band in the zonally asymmetric part of the midlatitude response, but there is a suggestion of a wave train arching across the North Pacific with a scale similar to the Pacific–North American (PNA) pattern (Wallace and Gutzler 1981). However, the simulated centers are displaced to the west of the observed PNA pattern. The integration would have to be extended to enhance the statistical significance of these extratropical patterns.

Associated patterns of sea level pressure and wind stress were found by correlating the NDJ average sea level pressure and zonal wind stress anomalies with the SST time series shown in Fig. 15. The correlation patterns for sea level pressure and wind stress associated with the mature tropical Pacific SST events are shown in Fig. 16. The wind stress anomalies are geostrophically consistent with the sea level pressure anomalies. Low sea level pressures in the eastern Pacific, high sea level pressures in the western Pacific and Indian Oceans, and westerly wind stress anomalies in the equatorial Pacific are associated with mature event warm SSTs in the eastern Pacific. The signs are reversed for cold SST anomalies. The sea level pressure pattern resembles the Southern Oscillation sea level pressure correlation pattern found from observations by Trenberth and Shea (1987, Fig. 1).

The Southern Oscillation index (SOI), based on the standardized Tahiti minus Darwin sea level pressure anomalies, was also calculated for the model simulation. The SOI (not shown) is strongly negatively correlated with the Nino3 (5°S–5°N, 150°–90°W) SST anomalies. However, comparison of Fig. 15 with Trenberth and Shea (1987, Fig. 1) shows that the simulated sea level pressure anomaly pattern is slightly shifted from the observed pattern so that Darwin lies very close to a nodal surface in the simulation. Then, the SOI as defined for observations is probably not the appropriate index for the model Southern Oscillation. The association of equatorial westerly wind stress anomalies with warm equatorial Pacific SST anomalies is a well-known re-

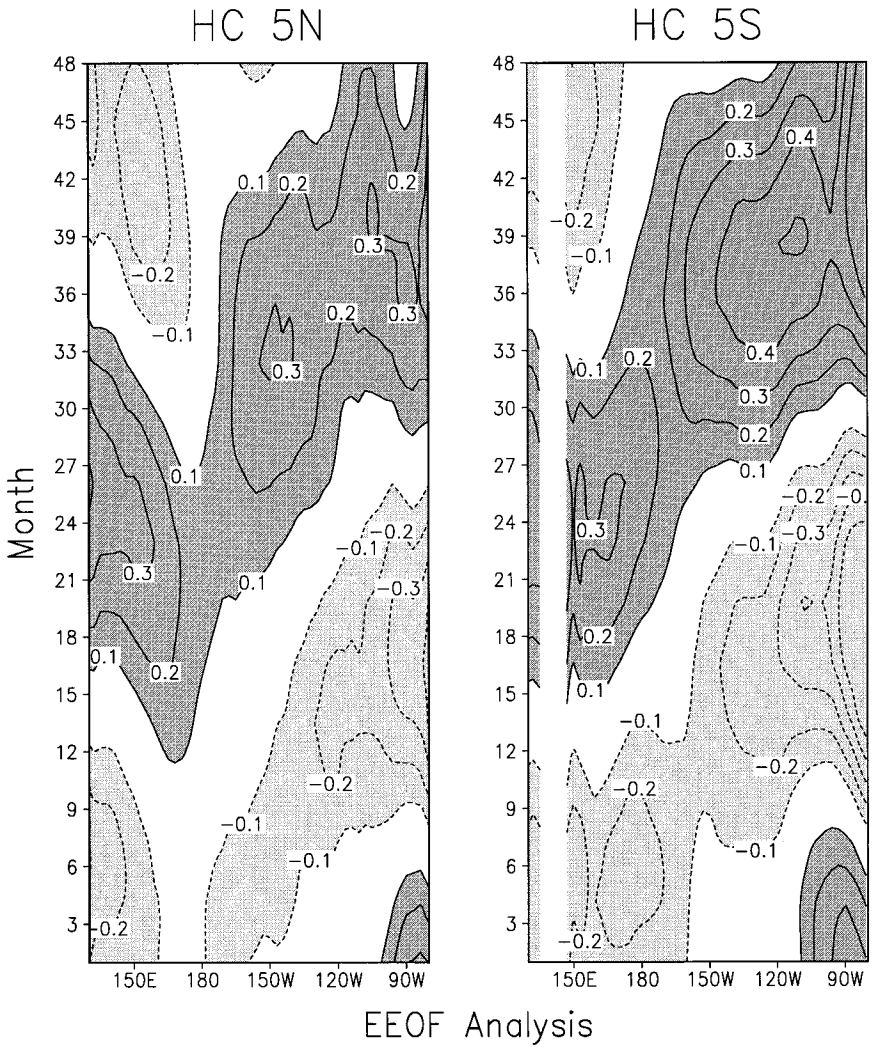

FIG. 14. Heat content (°C) from the extended empirical orthogonal function analysis described in the caption to Fig. 13. Left: heat content at 5°S. Right: heat content at 5°N. Contour interval 0.1°C, dashed contours negative. The vertical axis is time in months.

lationship. However, the strong correlation with anomalies of opposite sign near 10°S and 10°N found in the model are not associated with the observed El Niño (see Fig. 12, Huang and Schneider 1995).

The leading patterns from SVD analysis for the SST and precipitation fields in June–August (JJA) and NDJ are shown in Fig. 17. The JJA pattern explains 38% and the NDJ pattern explains 55% of the covariance for the respective seasons. Both patterns are for the warm, El Niño phase of the oscillation. Precipitation is enhanced in the central and eastern equatorial Pacific during the simulated El Niño. Precipitation is reduced in the rainy season in Australia, in India and southeast Asia in the summer monsoon, as well as northern South America and Central America, and eastern South Africa in NDJ. Precipitation is enhanced across Mexico and the Gulf of Mexico and southern India in NDJ, and equatorial Africa in JJA. The precipitation distributions in Fig. 17 agree remarkably well with the distribution of precipitation anomalies associated with El Niño developed by Ropelewski and Halpert (1987).

The leading pattern of the SVD analysis of NDJ 200-mb streamfunction and SST anomalies (not shown) explains 89% of the covariance and has the expected subtropical anticyclones in the central Pacific. Large anomalies also form at other longitudes in the Tropics, especially a cyclonic pair over the eastern Atlantic and Africa that is not directly related to the equatorial Pacific SST anomalies (also evident in the geopotential pattern in Fig. 15).

4. Summary

A multidecade integration of a coupled atmosphere–ocean general circulation model was conducted. The atmosphere was a coarse resolution R15, 18-level version

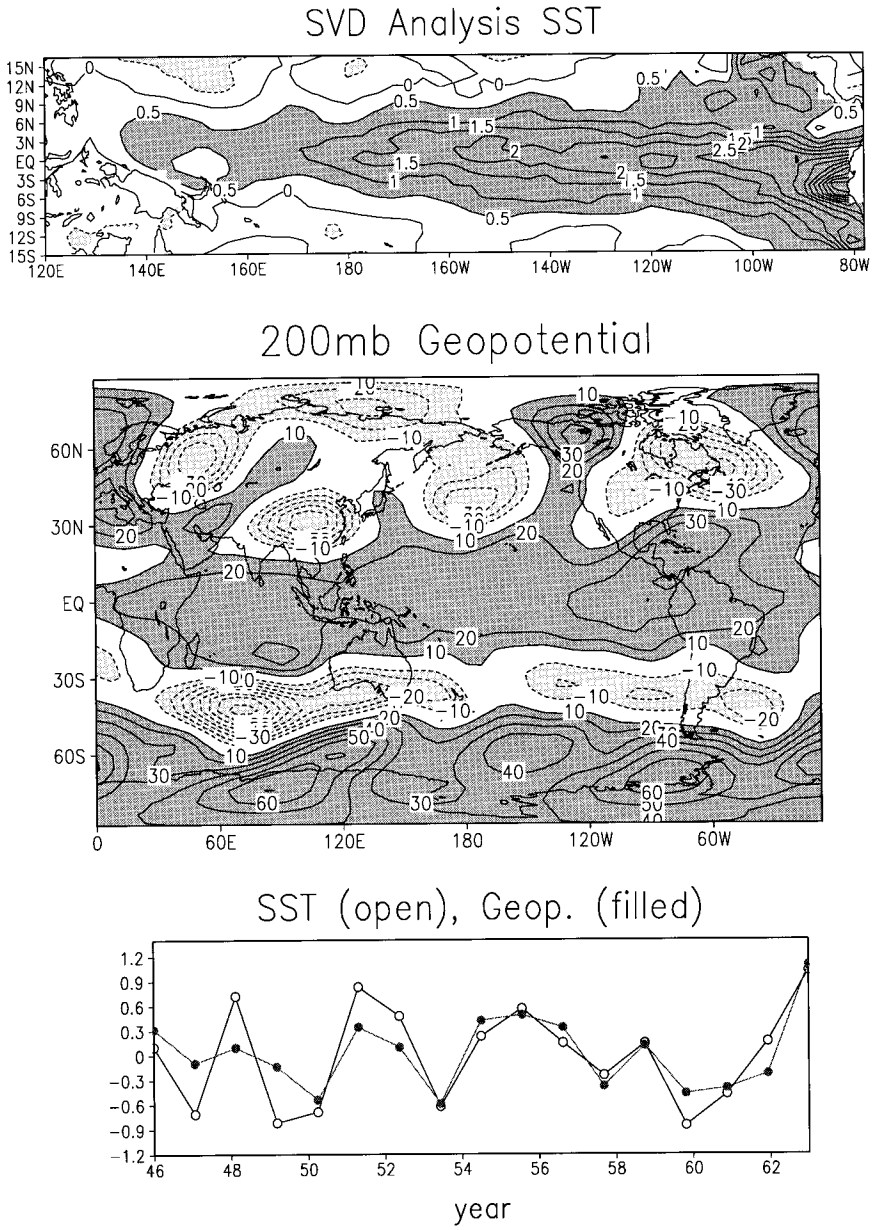

FIG. 15. Leading pattern resulting from an SVD analysis of November–January mean tropical Pacific SST and global 200-mb geopotential height from years 46–62 of the coupled integration. Top: SST pattern (°C), contour interval 0.5°C. Middle: 200-mb geopotential pattern (m), contour interval 10 m. Bottom: dimensionless time series for SST (open circles) and 200-mb geopotential (filled circles), with time axis in year of integration.

of the COLA AGCM. The ocean model was a medium resolution, equatorial waveguide resolving, nonpolar domain version of the GFDL MOM model. The coupling was direct: no flux corrections were applied.

Some adjustments were made to the AGCM cloud–radiation interaction schemes for cumulus towers and low-level stratus during the initial testing of the model to correct for deficiencies in the SST simulation. Convective cloudiness was decreased everywhere in order to increase the solar radiation reaching the surface and, hence, to increase the SST in the western equatorial Pacific. The stratus parameterization was improved to increase stratus cover, consequently reducing the solar radiation reaching the surface, and to decrease the SST in the eastern tropical Pacific. Both changes to the cloudiness had the expected effect on the solar radiation. However, the increased stratus also led to increased downward longwave radiation, which compensated for most of the stratus effect on the solar radiation. This compensation is probably unrealistic.

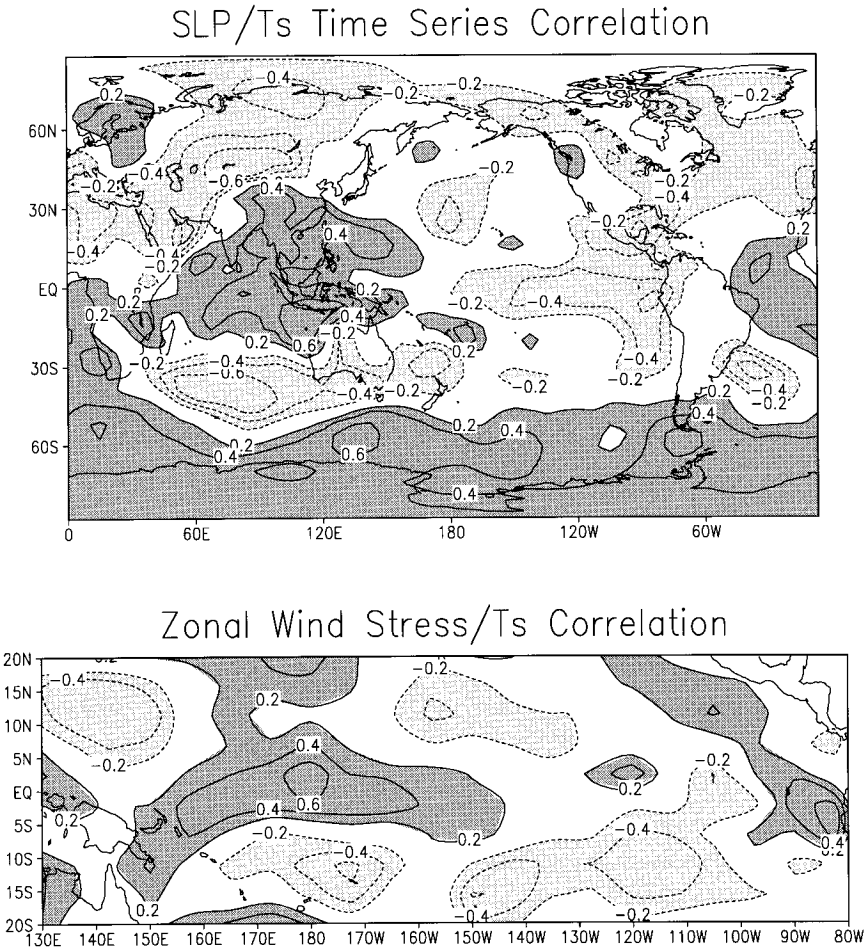

FIG. 16. Correlation of November–January sea level pressure anomalies (top) and tropical Pacific zonal wind stress anomalies (bottom) with SST time series shown in Fig. 12. Contour interval 0.2.

Coding errors were corrected after 16 and 25 years of model simulation. After 45 years of simulation, an empirical wind stress correction, extrapolating wind stress from the west to the near-equatorial South American coast, was introduced to try to improve the simulation of SSTs near the eastern boundaries of the Pacific and Atlantic basins. This correction had a positive effect, duplicating the response to the wind stress correction found in uncoupled simulations by Huang and Schneider (1995). However, the reduction of SST error near the coastline did not lead to improvement of SST away from the coast. This behavior leads us to conclude that the warm errors in SST in the eastern tropical Pacific and Atlantic are probably due to errors in the heat flux forcing of the ocean. The integration was suspended after 62 simulated years. The model appears to have spun up to a climatic equilibrium well before the last 17-yr period. This final period was therefore chosen for analysis.

The analysis concentrated on, but was not restricted to, the tropical Pacific. The ocean maintained a reasonably realistic east–west annual mean temperature gradient in the equatorial Pacific. However, due to the combined effects of an ocean model error of producing too narrow a tropical cold tongue and the low meridional resolution of the atmosphere, the atmosphere sees a much weaker equatorial Pacific east–west temperature gradient than produced by the ocean model. The effective equatorial coupling between the atmosphere and ocean models may be severely underestimated due to this problem.

The annual means simulated by the model had some realistic features and also serious deficiencies. The SST in the coupled model is realistic in the tropical western and central Pacific but is several degrees too warm near 10°S and 10°N in the eastern Pacific. The heat content is too small in the western and central Pacific, and much of the observed structure is not simulated. The east–west slope of the thermocline is small compared to observations in the equatorial Pacific, and the tropical Pacific thermocline depth is much more symmetrical about the equator than observed. Surface currents off the equator are much too weak. Many of these errors are closely associated with the problem of weak equatorial coupling and weak simulated wind stress.

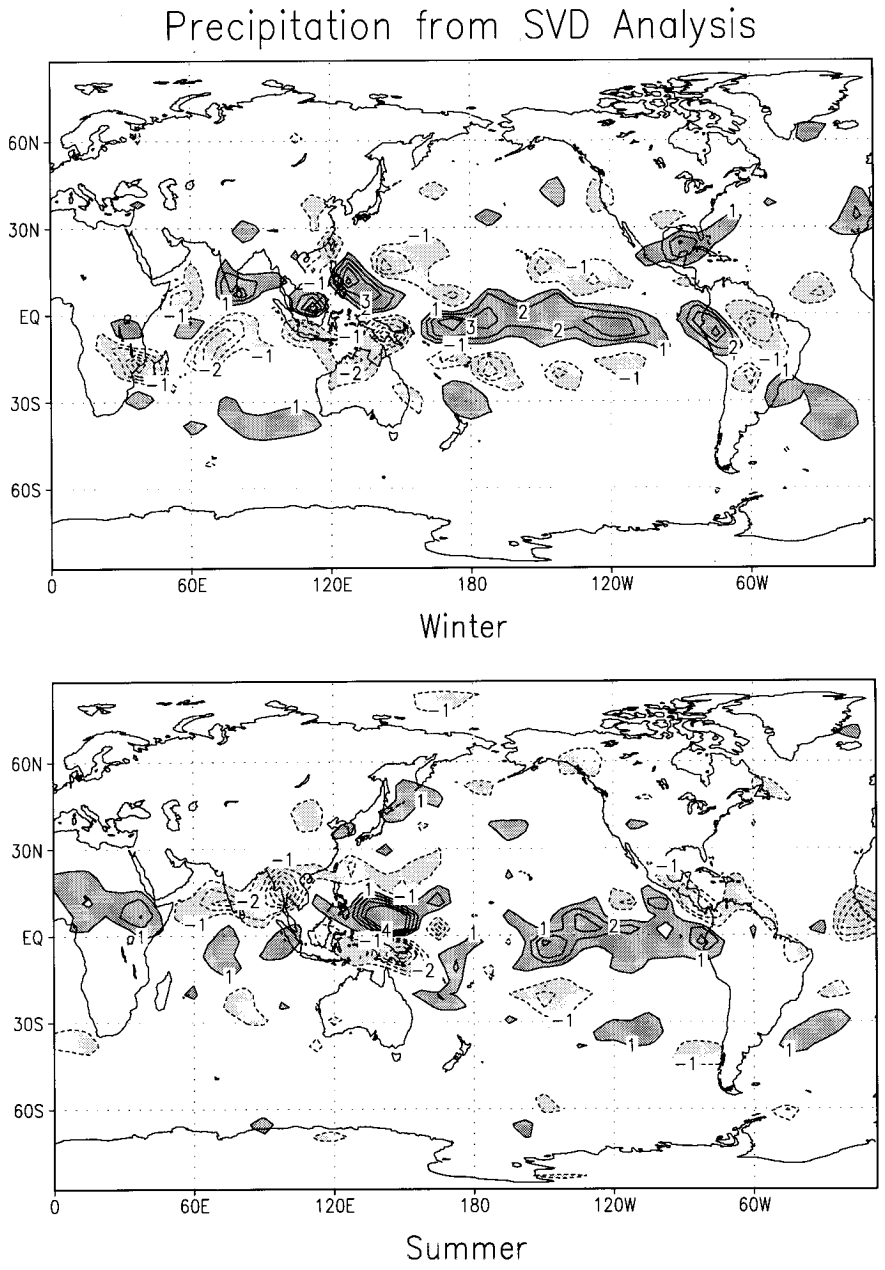

FIG. 17. Precipitation patterns (mm day^{-1}) resulting from SVD analysis of seasonal tropical Pacific SST and global precipitation. Top: analysis of November–January mean data. Bottom: analysis of June–August mean data. The SST pattern and time series is similar in both cases to those shown in Fig. 15, and the precipitation time series are positively correlated with the SST time series. Contour interval 1 mm day^{-1}, zero contour suppressed.

The model simulation of the annual cycle of SST in the equatorial Pacific gives the correct amplitude and phase except near the eastern boundary, where the amplitude is too small. The annual cycle of precipitation in the tropical Pacific simulates the main features except in March–May, when the simulated ITCZ disappears from north of the equator. The magnitude of the precipitation in the ITCZ north of the equator in other seasons is much weaker than observed. The simulated SPCZ forms too close to the equator in the eastern Pacific.

The simulated ENSO was examined using longitude–time sections of SST at the equator and heat content both on and off the equator, as well as by an EEOF analysis. Some features of the interannual variability in the tropical Pacific appear realistic. The typical warm or cold event in equatorial Pacific SST grows and decays

in place to an amplitude of about 1°C, about half of the observed typical amplitude, with little longitudinal propagation. The largest SST anomalies are confined to the eastern Pacific. The events alternate in sign and occur irregularly with a period of 3–6 yr. Heat content anomalies at the equator display systematic eastward propagation, taking about a year to cross the basin. The height of the SST events occur when the heat content anomalies of the same sign reach the eastern Pacific. Systematic westward propagation of heat content anomalies is found off the equator with phase speeds appropriate to Rossby waves. The relationships between heat content anomalies, SST, and wind stress are consistent with the delayed oscillator mechanism.

Some features of the tropical Pacific variability do not appear to be realistic. In particular, tropical heat content anomalies are too small near the western boundary relative to those in the eastern Pacific. The zonal wind stress does not appear to be not strong enough in the central Pacific relative to that near the eastern and western boundaries. The atmosphere and ocean appear to be too strongly coupled near the western boundary. It appears that the Rossby wave forcing associated with equatorial zonal wind stress anomalies is too weak relative to the forcing of the thermocline slope at the equator. The forcing error could result from atmospheric model meridional resolution that is too coarse near the equator. We will attempt in the future to isolate the specific aspects of the coupled model wind stress forcing responsible for the unrealistic heat content behavior using the conceptual model of the heat content response to the forcing discussed in Schneider et al. (1995).

Correlation and SVD analyses were used to isolate the global atmospheric component of the model ENSO. The sea level pressure pattern associated with a mature event is similar to that in the observed Southern Oscillation. Precipitation anomalies throughout the Tropics and subtropics resemble observed ENSO-related anomalies. The ENSO-related signal in the tropical upper-tropospheric geopotential appears realistic. There is an ENSO-related signal in the extratropical geopotential, but the number of simulated events analyzed is too small to unambiguously isolate the ENSO signal from that due to internal variability.

The results from this experiment suggest that a more realistic simulation of the annual and interannual variability of the tropical Pacific might be obtained by sufficiently increasing the tropical meridional resolution of the atmospheric component of the coupled atmosphere–ocean general circulation model. The atmospheric model needs to have sufficient meridional resolution at large zonal scales to be able to respond correctly to the primarily zonally aligned SST anomalies in a very narrow belt near the equator. The atmospheric model also needs to have sufficient meridional resolution to be able to produce a long, narrow, and vigorous primarily zonally aligned ITCZ some distance from the equator. The atmospheric model also needs sufficient meridional resolution to be able to correctly simulate the meridional gradients of the wind stress near the equator, which are important for forcing equatorial Rossby waves in the ocean. We note that the meridional resolution of large zonal scales in a spectral AGCM is superior for triangular truncation relative to rhomboidal truncation for the same number of spectral degrees of freedom. Therefore, we suggest that a spectral AGCM with triangular truncation should be preferred to one with rhomboidal truncation for coupled simulations of ENSO. However, the perceived requirement for enhanced atmospheric meridional resolution in this coupled GCM is partly due to problems inherent in the OGCM, especially the tendency to produce an excessively narrow equatorial cold tongue.

Acknowledgments. We gratefully acknowledge the contribution of model codes and personal assistance by A. Rosati and K. Miyakoda of GFDL in the development of our coupled model. Without their help, this work could not have been done. This work was supported under NOAA Grants NA26-GPO149 and NA46-GPO217, and NSF Grant ATM-93021354. Computer time for the coupled integration was provided through NOAA's Office of Global Programs.

REFERENCES

Alpert, J. C., M. Kanamitsu, P. M. Caplan, J. G. Sela, G. H. White, and E. Kalnay, 1988: Mountain induced gravity wave drag parameterization in the NMC medium-range forecast model. *Proc. Eighth Conf. on Numerical Weather Prediction,* Baltimore, MD, Amer. Meteor. Soc., 726–733.

Battisti, D. S., and A. C. Hirst, 1989: Interannual variability in a tropical atmosphere–ocean model: Influence of the basic state, ocean geometry, and nonlinearity. *J. Atmos. Sci.,* **46,** 1687–1712.

Bretherton, C. S., C. Smith, and J. M. Wallace, 1992: An intercomparison of methods for finding coupled patterns in climate data. *J. Climate,* **5,** 561–576.

Bryan, K., and L. Lewis, 1979: A water mass model of the world ocean. *J. Geophys. Res.,* **84,** 2503–2517.

Cane, M. A., and S. E. Zebiak, 1987: Prediction of El Niño events using a physical model. *Atmospheric and Oceanic Variability,* H. Cattel, Ed., Roy. Meteor. Soc., 153–182.

Chao, Y., and S. G. H. Philander, 1993: On the structure of the Southern Oscillation. *J. Climate,* **6,** 450–469.

ECMWF Research Department, 1988: *Research Manual 3. ECMWF Forecast Model Physical Parameterization*. European Centre for Medium-Range Weather Forecasts, 138 pp.

Fennessy, M. J., and Coauthors, 1994: The simulated Indian monsoon: A GCM sensitivity study. *J. Climate,* **7,** 33–43.

Goldenberg, S. B., and J. J. O'Brien, 1981: Time and space variability of the tropical Pacific wind stress. *Mon. Wea. Rev.,* **109,** 1190–1207.

Harshvardhan, R. Davies, D. A. Randall, and T. G. Corsetti, 1987: A fast radiation parameterization for atmospheric circulation models. *J. Geophys. Res.,* **92**(D1), 1009–1016.

Hou, Y.-T., 1990: Cloud–radiation–dynamics interactions. Ph.D. dissertation, University of Maryland at College Park, 209 pp.

Huang, B., and E. K. Schneider, 1995: The response of an ocean general circulation model to surface wind stress produced by an atmospheric general circulation model. *Mon. Wea. Rev.,* **123,** 3059–3085.

Ji, M., A. Kumar, and A. Leetmaa, 1994: An experimental coupled forecast system at the National Meteorological Center: Some early results. *Tellus,* **46A,** 398–418.

——, A. Leetmaa, and J. Derber, 1995: An ocean analysis system for seasonal to interannual climate studies. *Mon. Wea. Rev.,* **123,** 460–481.

Kinter, J. L., III, J. Shukla, L. Marx, and E. K. Schneider, 1988: A simulation of the winter and summer circulation with the NMC global spectral model. *J. Atmos. Sci.,* **45,** 2486–2522.

Kirtman, B. P., J. Shukla, B. Huang, Z. Zhu, and E. K. Schneider, 1997: Multiseasonal predictions with a coupled tropical ocean–global atmosphere system. *Mon. Wea. Rev.,* **125,** 789–808.

Kuo, H. L., 1965: On the formation and intensification of tropical cyclones through latent heat release by cumulus convection. *J. Atmos. Sci.,* **22,** 40–63.

Lacis, A. A., and J. E. Hansen, 1974: A parameterization for the absorption of solar radiation in the earth's atmosphere. *J. Atmos. Sci.,* **31,** 118–133.

Latif, M., A. Sterl, E. Maier–Reimer, and M. M. Junge, 1993: Climate variability in a coupled GCM. Part I: The tropical Pacific. *J. Climate,* **6,** 5–21.

——, T. Stockdale, J. Wolff, G. Burgers, E. Maier–Reimer, M. M. Junge, K. Arpe, and L. Bengtsson, 1994: Climatology and variability in the ECHO coupled GCM. *Tellus,* **46A,** 351–366.

Lau, N.-C., S. G. H. Philander, and M. J. Nath, 1992: Simulation of ENSO-like phenomena with a low-resolution coupled GCM of the global ocean and atmosphere. *J. Climate,* **5,** 284–307.

Levitus, S., 1982: *Climatological Atlas of the World Ocean*. U.S. Govt. Printing Office, 173 pp.

Manabe, S., and K. Bryan, 1969: Climate calculations with a combined ocean–atmosphere model. *J. Atmos. Sci.,* **26,** 786–789.

McCarty, M. E., and M. J. McPhaden, 1993: Mean seasonal cycles and interannual variations at 0°, 165°E during 1986–1992. NOAA Tech. Memo. ERL PMEL-98, 64 pp. [Available from U.S. Dept. of Commerce Pacific Marine Environmental Laboratory, 7600 Sand Point Way, N.E., Seattle, WA 98115.]

McPhaden, M. J., and M. E. McCarty, 1992: Mean seasonal cycles and interannual variations at 0°, 110°W and 0°, 140°W during 1980–1991. NOAA Tech. Memo. ERL PMEL-95, 118 pp. [Available from U.S. Dept. of Commerce Pacific Marine Environmental Laboratory, 7600 Sand Point Way, N.E., Seattle, WA 98115.]

Mechoso, C. R., and Coauthors, 1995: The seasonal cycle over the tropical Pacific in coupled ocean–atmosphere general circulation models. *Mon. Wea. Rev.,* **123,** 2825–2838.

Mellor, G. L., and T. Yamada, 1982: Development of a turbulence closure model for geophysical fluid processes. *Rev. Geophys. Space Phys.,* **20,** 851–875.

Miyakoda, K., and J. Sirutis, 1977: Comparative integrations of global spectral models with various parameterized processes of subgrid scale vertical transports. *Beitr. Phys. Atmos.,* **50,** 445–447.

Nagai, T., T. Tokioka, M. Endoh, and Y. Kitamura, 1992: El Niño–Southern Oscillation simulated in an MRI atmosphere–ocean coupled general circulation model. *J. Climate,* **5,** 1202–1233.

Neelin, J. D., and Coauthors, 1992: Tropical air–sea interaction in general circulation models. *Climate Dyn.,* **7,** 73–104.

Pacanowski, R., and S. G. H. Philander, 1981: Parameterization of vertical mixing in numerical models of tropical oceans. *J. Phys. Oceanogr.,* **11,** 1443–1451.

Philander, S. G. H., R. C. Pacanowski, N.-C. Lau, and M. J. Nath, 1992: Simulation of ENSO with a global atmospheric GCM coupled to a high-resolution, tropical Pacific Ocean GCM. *J. Climate,* **5,** 308–329.

Phillips, N. A., 1957: A coordinate system having some special advantages for numerical forecasting. *J. Meteor.,* **14,** 184–185.

Robertson, A. W., C.-C. Ma, C. R. Mechoso, and M. Ghil, 1995a: Simulation of the tropical Pacific climate with a coupled ocean–atmosphere general circulation model. Part I: The seasonal cycle. *J. Climate,* **8,** 1178–1198.

——, ——, M. Ghil, and C. R. Mechoso, 1995b: Simulation of the tropical Pacific climate with a coupled ocean–atmosphere general circulation model. Part II: Interannual variability. *J. Climate,* **8,** 1199–1216.

Ropelewski, C. F., and M. S. Halpert, 1987: Global and regional scale precipitation associated with El Niño/Southern Oscillation. *Mon. Wea. Rev.,* **115,** 1606–1626.

——, J. E. Janowiak, and M. S. Halpert, 1985: The analysis and display of real time surface climate data. *Mon. Wea. Rev.,* **113,** 1101–1107.

Sato, N., P. J. Sellers, D. A. Randall, E. K. Schneider, J. Shukla, J. L. Kinter III, Y.-T. Hou, and E. Albertazzi, 1989a: Effects of implementing the simple biosphere model (SiB) in a general circulation model. *J. Atmos. Sci.,* **46,** 2752–2782.

——, ——, ——, ——, ——, ——, ——, and ——, 1989b: Implementing the simple biosphere model (SiB) in a general circulation model: Methodology and results. NASA Contractor Rep. NASA CR-185509, 80 pp. [Available from National Technical Information Service, Springfield, VA 22161.]

Schneider, E. K., 1984: Response of the annual and zonal mean winds and temperatures to variation in the heat and momentum sources. *J. Atmos. Sci.,* **41,** 1093–1115.

——, 1987: A simplified model of the modified Hadley circulation. *J. Atmos. Sci.,* **44,** 3311–3328.

——, and J. L. Kinter III, 1994: An examination of internally generated variability in long climate simulations. *Climate Dyn.,* **10,** 181–204.

——, B. Huang, and J. Shukla, 1995: Ocean wave dynamics and El Niño. *J. Climate,* **8,** 2415–2439.

Schopf, P. S., and M. J. Suarez, 1988: Vacillations in a coupled ocean–atmosphere model. *J. Atmos. Sci.,* **45,** 549–566.

Sela, J. G., 1980: Spectral modeling at the National Meteorological Center. *Mon. Wea. Rev.,* **108,** 1279–1292.

Sellers, P. J., Y. Mintz, Y. C. Sud, and A. Dalcher, 1986: A simple biosphere model (SiB) for use within general circulation models. *J. Atmos. Sci.,* **43,** 505–531.

Slingo, J. M., 1987: The development and verification of a cloud prediction scheme for the ECMWF model. *Quart. J. Roy. Meteor. Soc.,* **113,** 899–927.

Spencer, R., 1993: Global oceanic precipitation from the MSU during 1979–1991 and comparisons to other climatologies. *J. Climate,* **6,** 1301–1326.

Stockdale, T., M. Latif, G. Burgers, and J.-O. Wolff, 1994: Some sensitivities of a coupled ocean–atmosphere GCM. *Tellus,* **46A,** 367–380.

Suarez, M. J., and P. S. Schopf, 1988: A delayed action oscillator for ENSO. *J. Atmos. Sci.,* **45,** 3283–3287.

Tiedtke, M., 1984: The effect of penetrative cumulus convection on the large-scale flow in a general circulation model. *Beitr. Phys. Atmos.,* **57,** 216–239.

Trenberth, K. E., and D. J. Shea, 1987: On the evolution of the Southern Oscillation. *Mon. Wea. Rev.,* **115,** 3078–3096.

Vernekar, A., B. Kirtman, J. Zhou, and D. DeWitt, 1992: Orographic gravity-wave drag effects on medium-range forecasts with a general circulation model. *Physical Processes in Atmospheric Models,* D. R. Sikka and S. S. Singh, Eds., Wiley Eastern Limited, 295–307.

Wallace, J. M., and D. S. Gutzler, 1981: Teleconnections in the geopotential height field during the Northern Hemisphere winter. *Mon. Wea. Rev.,* **109,** 784–812.

Weare, B. C., and J. S. Nasstrom, 1982: Examples of extended empirical orthogonal function analysis. *Mon. Wea. Rev.,* **110,** 481–485.

Xue, Y., P. J. Sellers, J. L. Kinter III, and J. Shukla, 1991: A simplified model for global climate studies. *J. Climate,* **4,** 345–364.